

Capture and transmission of
signal data from infrared detectors
using a microcontroller and
graphical display of received data
in a Windows environment

Bachelor's Thesis in the Bachelor Degree Programme
Electrical Engineering / Information Technology^{plus}

Sebastian Frei

University of Applied Sciences Offenburg
Faculty of Electrical Engineering and Information Technology
Edinburgh Napier University
School of Engineering and Built Environment

August 24, 2009

Thesis Supervisors:
Dr. T. David Binnie
Prof. Dr. rer. nat. Christoph Nachtigall

Abstract

This report details the development of an experimental kit to detect infrared radiation, emitted by a human.

The experimental kit consists of four sensor boxes, one microcontroller and a computer software. The sensor boxes detect the infrared radiation and transform it in an analogue output signal. These signals are digitalized by a microcontroller to send them to a computer. The computer represents the signals in a chart.

These detected signals can be analysed in further investigations to implement intelligent algorithms to detect people. Human detection can be used for control purposes, the control of the lights in a room for example.

Acknowledgements

This study is based on the research work at the Edinburgh Napier University in the School of Engineering and Built Environment.

I greatly enjoyed my time in Edinburgh and would like to thank Dr. T. David Binnie and Mr. Murray MacCallum from the Edinburgh Napier University, the International Office and Prof. Dr. rer. nat. Christoph Nachtigall from the University of Applied Sciences Offenburg, all of whom made it possible for me to write my thesis in Scotland.

I would like to thank Dr. T. David Binnie for taking the time to make me feel welcome and for many interesting conversations about both this project and other shared interests.

I would like to thank Prof. Dr. rer. nat. Christoph Nachtigall for his continued support via telephone and email.

I gratefully acknowledge the financial support from the Thomas Gessmann-Stiftung im Stifterverband für die Deutsche Wissenschaft.

I shared an office with Robert Walczyk and would like to thank him for our wide-ranging daily discussions.

I would like to thank Jim Hammond, Nathan Gove and especially Paul Sleggs for correcting the errors in my written English.

Sebastian Frei <info@s-frei.de>

Declaration

I declare that this thesis was composed by me, that the work contained herein is my own except where explicitly stated otherwise in the text, and that this work has not been submitted for any other degree or professional qualification except as specified.

Edinburgh, August 24, 2009

Sebastian Frei

Contents

Contents	IV
List of Tables	VI
List of Figures	VII
1 Introduction	10
2 Thermal radiation	11
2.1 The Electromagnetic Spectrum	11
2.2 Infrared radiation	13
2.3 Black Body radiation	13
2.4 Emissivity	15
2.5 Radiation emitted by human skin	18
3 Detectors for infrared radiation	20
3.1 Thermal detectors	20
3.2 The pyroelectric effect	20
3.3 Pyroelectric detectors	22
3.3.1 Thermal conversion	22
3.3.2 Thermal to electrical conversion	23
3.3.3 Electrical conversion	24
3.3.4 Compensation	24
3.4 Optical system	25
3.4.1 Fresnel lens for incident radiation	25
3.4.2 Relation between the person and the sensor output frequency	25
4 Electrical Filters	28
4.1 High pass filter	28

CONTENTS

4.2	Band pass filter	29
4.2.1	Inverted band pass filter	29
4.2.2	Non inverted band pass filter	30
5	Proposed design	33
5.1	Capture of signal data	34
5.1.1	Fresnel lens	34
5.1.2	Dual Element Detector LHi 958	35
5.1.3	Sensor board schematic	37
5.1.4	V0 sensor board layout	44
5.1.5	V0 sensor board hardware test	46
5.1.6	V1 sensor board layout	48
5.1.7	V1 sensor board hardware test	49
5.1.8	Final sensor board circuit with lens in a package	50
5.2	Transmission of signal data	52
5.2.1	Microcontroller Development Kit	53
5.2.2	Microcontroller C8051F350	54
5.2.3	24 bit analogue to digital converter	55
5.2.4	Universal asynchronous receiver/transmitter	60
5.2.5	Implemented Firmware on the microcontroller	62
5.3	Graphical display in a Windows environment	65
5.3.1	Connection to serial port	65
5.3.2	Microsoft chart controls	66
5.3.3	Software functionality	66
6	Sample applications	69
6.1	Output signal of one sensor box	69
6.2	Output signal of four sensor boxes	74
7	Conclusion	78
	Bibliography	79

List of Tables

2.1	Sub regions of the infrared spectrum	13
2.2	Emissivity ϵ of different materials	17
3.1	Pyroelectric coefficient p of some materials	21
5.1	Pin configuration from the connector in the sensor box	51
5.2	ADC0MUX register values from the microcontroller to configure the multiplexer	56
5.3	D-byte values including the state of digital inputs P1.0 and P0.0	63
5.4	After a microcontroller reset the microcontroller waits for a byte on the UART0 serial port to set the number of analogue inputs. This table contains the accepted values for this byte.	63
5.5	While the microcontroller sends frames to the computer the microcontroller can be reset or the digital output P0.6 can be toggled. The accepted byte values on UART0 are shown in this table	64

List of Figures

2.1	The electromagnetic spectrum between the wavelength $\lambda = 10^{-16} m$ and $\lambda = 10^4 m$	11
2.2	An electromagnetic wave travelling in the propagation direction z	12
2.3	Spectral radiant emittance W_λ from the 'Black body' at temperatures between $700 K \leq T \leq 900 K$ calculated with Plank's law.	15
2.4	Spectral radiant emittance W_λ of 'Black body' at temperatures between $280 K \leq T \leq 320 K$	18
3.1	Pyroelectric element with electrodes while change in temperature	21
3.2	Conversion stages of the pyroelectric infrared detector	22
3.3	Simplified thermal model from a pyroelectric detector	23
3.4	Electrical circuit from the simplified thermal model of the pyroelectric detector	23
3.5	Voltage follower realized with an ideal operational amplifier	24
3.6	Current follower realized with an ideal operational amplifier	24
3.7	Compensation of the pyroelectric sensing element with a second pyroelectric sensing element. They are oppositely connected and one of them is isolated against incident radiation	25
3.8	Graphic example for a Fresnel lens on the left and a normal lens on the right. Both have the same focal length	26
3.9	Optical system between the person and the sensing element with a Fresnel lens. Variables: Walking velocity v_b , output frequency f_{sens} , sensing element size s , focal length f_b .	27
4.1	High pass filter with the passive components resistor R and capacitor C	28
4.2	Amplitude transfer function versus frequency for a high pass filter with $C = 47 \mu F$ and $R = 1 M\Omega$. The dotted line represents the 3 dB cut off frequency f_c	29
4.3	Inverted amplifier circuit with an operational amplifier and external components	30
4.4	An operational amplifier with discrete components. The circuit acts as a inverted band pass filter with amplification	30

LIST OF FIGURES

4.5	Non inverted amplifier circuit with an operational amplifier and external components	31
4.6	An operational amplifier with discrete components. The circuit acts as a non inverted band pass filter with amplification	31
4.7	Amplitude transfer function versus frequency for a non inverted band-pass filter with an ideal operational amplifier and discrete components	32
5.1	Flow chart from the proposed experimental kit. A person emits infrared radiation. This radiation is detected with four sensor boxes. The computer software plots the output signal from the sensor boxes in a chart.	33
5.2	Transmittance τ of POLY IR 2 material as a function of the wavelength λ . Thickness = 0.38 mm	34
5.3	Sensor output signal generated by a person moving from the left to the right . .	35
5.4	Dual element detector LHi 958	35
5.5	Responsivity versus frequency from dual element detector LHi 958	36
5.6	Signal flow chart for board schematic	37
5.7	Schematic diagram of amplification and band pass Filter for infrared sensor LHi 958 in Eagle 5.6.0	39
5.8	Amplitude response from board circuit simulated with Tina	42
5.9	Phase response from board circuit simulated with Tina	42
5.10	Time signal stages from board schematic with $V_{in} = 800 mV + 10 mV \cdot \sin(2\pi \cdot 5 Hz \cdot t)$	43
5.11	v0 sensor board layout for signal conditioning of infrared sensor LHi 958	44
5.12	Photo from the top of the v0 sensor board	45
5.13	Photo from the bottom of the v0 sensor board	45
5.14	Test assembly for the hardware test for the sensor board	46
5.15	Photo from test assembly of the v0 board	46
5.16	Amplitude transfer response from the v0 board	47
5.17	V1 sensor board layout for signal conditioning of infrared sensor LHi 958 in Eagle 5.6.0	48
5.18	Photo from the top of the v1 sensor board	48
5.19	Photo from the bottom of the v1 sensor board	48
5.20	Amplitude transfer response from the v1 sensor board	49
5.21	Photo from the dual element detector Lhi 958, the lens and the v1 sensor board	50
5.22	Photo from the opened sensor box	50
5.23	Photo from the sensor box with connector and lens from outside	51

LIST OF FIGURES

5.24	Targeted Board from the development kit C8051F350DK from Silicon Labs	53
5.25	Connections for the multiplexer from the analogue to digital converter	55
5.26	Analogue to digital converter ADC0 block diagram	57
5.27	Operating states for single conversion mode with various analogue input signals	59
5.28	RS-232 connection between the PC and the microcontroller	61
5.29	8-Bit UART mode bit sampling	61
5.30	RS-232 frame for one digitized value	62
5.31	RS-232 frame for four digitized values	62
5.32	Signal from a person moving from the right to the left side. The areas A1, A2 and A3 are the detected areas. The software integrates about the detected areas.	68
6.1	Signal from a person moving down the sensor box with a walking speed $v_b =$ $1.2 \frac{m}{s}$. The working distance between the person and the sensing box is $L =$ 90 cm . The graph shows <i>voltage / mV</i> versus <i>time / 15 ms</i>	71
6.2	Signal from a person moving down the sensor box with a walking speed $v_b =$ $1.8 \frac{m}{s}$. The working distance between the person and the sensing box is $L =$ 90 cm . The graph shows <i>voltage / mV</i> versus <i>time / 15 ms</i>	72
6.3	Signal from a person moving down the sensor box with a walking speed $v_b =$ $2.1 \frac{m}{s}$. The working distance between the person and the sensing box is $L =$ 90 cm . The graph shows <i>voltage / mV</i> versus <i>time / 15 ms</i>	73
6.4	Output signal from four sensor boxes while a person walks with a walking speed $v_b = 0.8 \frac{m}{s}$. The distance between two sensor boxes is $s_1 = 1.1 \text{ m}$. The graph shows <i>voltage / mV</i> versus <i>time / 15 ms</i>	75
6.5	Output signal from four sensor boxes while a person walks with a walking speed $v_b = 1.2 \frac{m}{s}$. The distance between two sensor boxes is $s_1 = 1.1 \text{ m}$. The graph shows <i>voltage / mV</i> versus <i>time / 15 ms</i>	76
6.6	Output signal from four sensor boxes while a person walks with a walking speed $v_b = 4.5 \frac{m}{s}$. The distance between two sensor boxes is $s_1 = 1.1 \text{ m}$. The graph shows <i>voltage / mV</i> versus <i>time / 15 ms</i>	77

1 Introduction

Each person emits infrared radiation which is related to the temperature of the human skin. This document describes the basics about thermal radiation, detectors of this radiation and electrical filters. Furthermore an experimental kit with four infrared sensors has been developed. This experimental kit can be connected to a computer to display the signals in a Windows environment. Finally some signals are recorded and analysed with the experimental kit software while a person crosses the detection area.

The experimental kit consists of four infrared sensor boxes, one microcontroller and software for the computer.

Each infrared sensor box consists of a dual element detector and an electric circuit. The dual element detector transforms the incident infrared radiation into an electrical signal and the electric circuit amplifies and filters this signal.

The signals from the infrared sensor boxes are transmitted to the microcontroller. This digitises the signals and sends them via a serial port to the computer. The computer runs an application to represent the signals in a chart.

In further investigations these signals can be used to implement algorithms to detect and track people.

2 Thermal radiation

This chapter describes the thermal radiation emitted by human skin and their location in the electromagnetic spectrum. Furthermore the 'Black body' and the emissivity ε are described.

2.1 The Electromagnetic Spectrum

In everyday life there are many different types of electromagnetic radiation, for example sunlight, mobile phone waves and heat. All these different types of radiation are divided into parts of the electromagnetic spectrum. The radiation is characterised by the wavelength λ or frequency ν . The visible part for our eyes has a wavelength between about $0.4 \mu\text{m}$ and $0.75 \mu\text{m}$ [1]. Out of this range there are many other regions which are not visible to us. Figure 2.1 shows the electromagnetic spectrum between the wavelength $\lambda = 10^{-16} \text{ m}$ and $\lambda = 10^4 \text{ m}$.

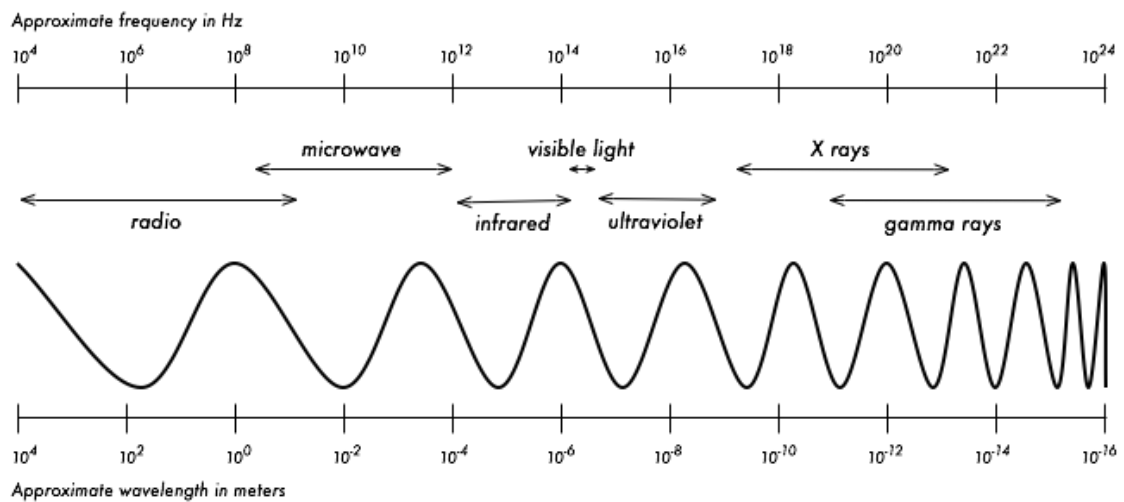


Figure 2.1: The electromagnetic spectrum between the wavelength $\lambda = 10^{-16} \text{ m}$ and $\lambda = 10^4 \text{ m}$ [2]

2 Thermal radiation

The theories of Maxwell describe the wave nature of electromagnetic radiation. According to it, waves are composed of a magnetic and an electric field oscillation. The changing magnetic field causes a change in the electrical field which causes again a change in the magnetic field and so on. Both, magnetic and electric field are oriented perpendicular to each other. Figure 2.2 shows the electromagnetic wave propagation with a magnetic wave M and an electric wave E . Both of them build the electromagnetic wave which is travelling in the positive direction z . All these waves have the same propagation velocity $c = 3 \cdot 10^8 \frac{m}{s}$ in a vacuum. The relation between wavelength λ in vacuum, the frequency ν and propagation velocity c is described by Equation 2.1.

$$\lambda = \frac{c}{\nu} \quad (2.1)$$

where

λ = wavelength, m

c = propagation velocity of light $c = 2.997925 \cdot 10^8 \frac{m}{s}$

ν = frequency, Hz.

The wavelength is the distance between two consecutive points of a wave that has the same phase in direction of propagation.

To characterise a wave it is common to use wavelength λ or frequency ν which depends on the application. For mobile phones the frequency such as $\nu = 900 \text{ MHz}$ is used and for infrared radiation the wavelength such as $\lambda = 10 \mu\text{m}$ is used.

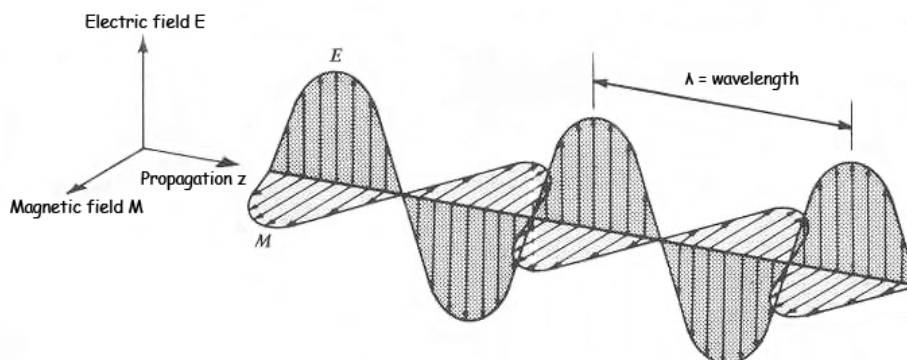


Figure 2.2: An electromagnetic wave travelling in the propagation direction z

2.2 Infrared radiation

The infrared spectrum is defined at a wavelength range between $\lambda = 0.75 \mu m$ and $\lambda = 1000 \mu m$ which is given in Equation 2.2.

$$0.75 \mu m < \lambda < 1000 \mu m \quad (2.2)$$

The infrared region is separated into different sub regions which are shown in Table 2.1.

Designation	Limits
Near infrared	0.75 μm to 3 μm
Middle infrared	3 μm to 6 μm
Far infrared	6 μm to 15 μm
Extreme infrared or sub-millimetre	15 μm to 1000 μm

Table 2.1: Sub regions of the infrared spectrum [3]

The division in sub-regions is based on different criteria such as the classification of radiation detectors, the equipment used for the spectral decomposition of the radiation or the radiation transmission in the atmosphere.

2.3 Black Body radiation

Part of radiation falling on an objects surface will be absorbed, α ($\alpha = \frac{P_{absorbed}}{P_{irradiate}}$). A part will be transmitted, τ ($\tau = \frac{P_{transmitted}}{P_{irradiate}}$). A part will be reflected, ρ ($\rho = \frac{P_{reflected}}{P_{irradiate}}$). A body that doesn't transmit and reflect radiation ($\tau = \rho = 0$) is called 'Black body'. This theoretical body absorbs all radiation ($\alpha = 1$). However the 'Black body' emits a temperature dependent spectrum of radiation. The spectral distribution of the radiation from a 'Black body' is explained with Planck's law in Equation 2.3.

$$W_\lambda = \frac{2\pi hc^2}{\lambda^5} \frac{1}{e^{\frac{hc}{\lambda kT}} - 1} \quad (2.3)$$

2 Thermal radiation

Plank's law can be written as

$$W_\lambda = \frac{c_1}{\lambda^5} \frac{1}{e^{\frac{c_2}{\lambda T}} - 1} \quad (2.4)$$

where

$$\begin{aligned} W_\lambda &= \text{spectral radiant emittance, } \frac{W}{cm^2 \mu m} \\ T &= \text{absolute temperature, } K \\ \lambda &= \text{wavelength, } \mu m \\ h &= \text{Planck's constant} = 6.6256 \cdot 10^{-34} \frac{W}{s^2} \\ c &= \text{velocity of light} = 2.997925 \cdot 10^8 \frac{m}{s} \\ c_1 &= 2\pi h c^2 = 3.7415 \cdot 10^{-16} W m^2 \\ c_2 &= \frac{ch}{k} = 1.43879 \cdot 10^{-2} mK \\ k &= \text{Boltzmann's constant} = 1.38054 \cdot 10^{-23} \frac{Ws}{K}. \end{aligned}$$

The spectral radiant emittance W_λ describes the radiant emittance W within a spectral interval $\Delta\lambda$ wide, radiated into a hemisphere by a 'Black body'. The radiant emittance W is the power per unit area of electromagnetic radiation at a surface.

Absolute zero is at $T = 0 K = -273.15 \text{ }^\circ C$. The relationship between $^\circ C$ and K is given in Equation 2.5.

$$T_{^\circ C} = (T_K - 273.15 K) \frac{^\circ C}{K} \quad (2.5)$$

where

$$\begin{aligned} T_{^\circ C} &= \text{Temperature, } ^\circ C \\ T_K &= \text{Temperature, } K. \end{aligned}$$

The emitted spectrum's from a 'Black body' at temperatures between $T = 700 K$ and $T = 900 K$ are shown in Figure 2.3. These diagrams are calculated with Plank's Law. The peak at each spectral curve can be calculated by solving the maximum of Plank's law and gives Wien's displacement law, shown in Equation 2.6.

$$\lambda_m T = \alpha \quad (2.6)$$

where

$$\begin{aligned} \lambda_m &= \text{wavelength at maximum spectral radiant emittance, } m \\ \alpha &= 2897.8 \mu m K \\ T &= \text{absolute object temperature, } K. \end{aligned}$$

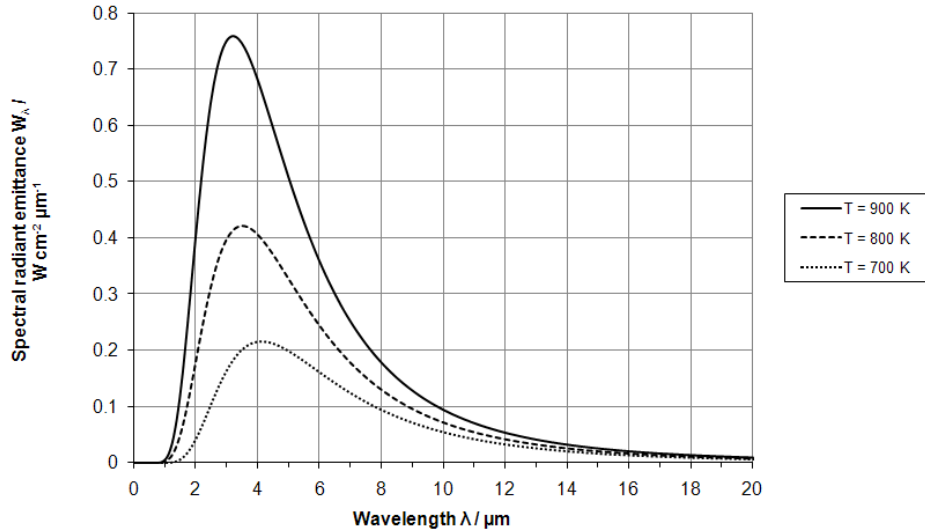


Figure 2.3: Spectral radiant emittance W_λ from the 'Black body' at temperatures between $700\text{ K} \leq T \leq 900\text{ K}$ calculated with Planck's law.

Wavelength λ_m at maximum spectral radiant emittance for absolute temperatures T in Figure 2.3, calculated with Wien's displacement law is:

$$\lambda_m(900\text{ K}) = \frac{2897.8\ \mu\text{mK}}{900\text{ K}} = 3.2\ \mu\text{m} \quad (2.7)$$

$$\lambda_m(800\text{ K}) = \frac{2897.8\ \mu\text{mK}}{800\text{ K}} = 3.6\ \mu\text{m} \quad (2.8)$$

$$\lambda_m(700\text{ K}) = \frac{2897.8\ \mu\text{mK}}{700\text{ K}} = 4.1\ \mu\text{m} \quad (2.9)$$

With the decrease of the temperature T the wavelength for the maximum value from the spectral radiant emittance λ_m increases.

2.4 Emissivity

Planck's law describes the spectral radiant emittance W_λ at different wavelengths λ . The integration, about the wavelength limits extending from zero to infinity, gives the radiant emittance W , which describes the flux radiated into the hemisphere above a 'Black body' with a surface area A . Solving this integral produces the Stefan-Boltzmann law, given in

2 Thermal radiation

Equation 2.10.

$$W = \frac{2\pi^5 k^4}{15c^2 h^3} T^4 = \sigma T^4 \quad (2.10)$$

where

$$\begin{aligned} W &= \text{radiant emittance, } \frac{W}{\text{cm}^2} \\ \sigma &= \text{Stefan-Boltzmann constant} = 5.6698 \cdot 10^{-12} \frac{W}{\text{cm}^2 K^4} \end{aligned}$$

Only a 'Black body' with a absolute temperature $T = 0 \text{ K}$ emits no radiation. At all other temperatures, except for $T = 0 \text{ K}$, the 'Black body' emits temperature related radiation. The radiant emittance W increases with the forth power of the absolute temperature T as given in Equation 2.10. Small increases in temperature T cause high increases in radiant emittance W . Radiant emittance W is used to describe the radiant emittance from a 'Black body'. To describe the radiant emittance W' of any object emissivity ϵ is used. The emissivity ϵ describes the ratio of radiant emittance W' of an object to the theoretical radiant emittance W of the 'Black body' at the same temperature.

$$\epsilon = \frac{W'}{W} \quad (2.11)$$

A non radiating source has an emissivity ϵ of zero and a 'Black body' has a emissivity ϵ of unity. The numeric value of ϵ can be between zero and unity. Many real objects have similar radiation characteristics as a 'Black body'. It is easy to construct a furnace which emits at $T_K = 900 \text{ K}$ most radiation at about $3 \mu\text{m}$ [4]. The calculation for the wavelength at maximum spectral radiant emittance from a 'Black body' with Wien's displacement law gets the result:

$$\lambda_m(900 \text{ K}) = \frac{2897.8 \mu\text{mK}}{900 \text{ K}} = 3.2 \mu\text{m} \quad (2.12)$$

This theoretical wavelength peak for the 'Black body' is very close to the real emitted wavelength peak from this object. Various materials, see Table 2.2, have radiant characteristics like a 'Black body' and therefore a emissivity ϵ close to unity. Materials with emissivity ϵ close to unity can be approximated with Planck's law as a 'Black body'.

Material	Temperature $T_{\circ C}/^{\circ}C$	Emissivity ϵ
Polished aluminium sheet	100	0.05
Polished copper	100	0.05
Distilled water	20	0.96
Snow	-10	0.85
Skin, human	32	0.98
White bond paper	20	0.93
Polished glass plate	20	0.94

Table 2.2: Emissivity ϵ of different materials [3]

2.5 Radiation emitted by human skin

Human skin radiates between the wavelength $\lambda = 5 \mu m$ and $\lambda = 10 \mu m$ nearly as a 'Black body' [5]. The exact value for the emissivity ϵ for human skin at a temperature $T_{\circ C} = 32 \text{ }^{\circ}C$ is $\epsilon = 0.98$, according to Table 2.2 on page 17, which accounts that human skin radiates nearly as a 'Black body' for body temperature. In Figure 2.4 is the spectral radiant emittance W of a 'Black body' at temperatures between $T = 280 K = 6,85 \text{ }^{\circ}C$ and $T = 320 K = 46,85 \text{ }^{\circ}C$, to demonstrate the 'Black body' spectrum at skin temperature. The skin temperature is around $T = 33 \text{ }^{\circ}C = 306.1 K$.

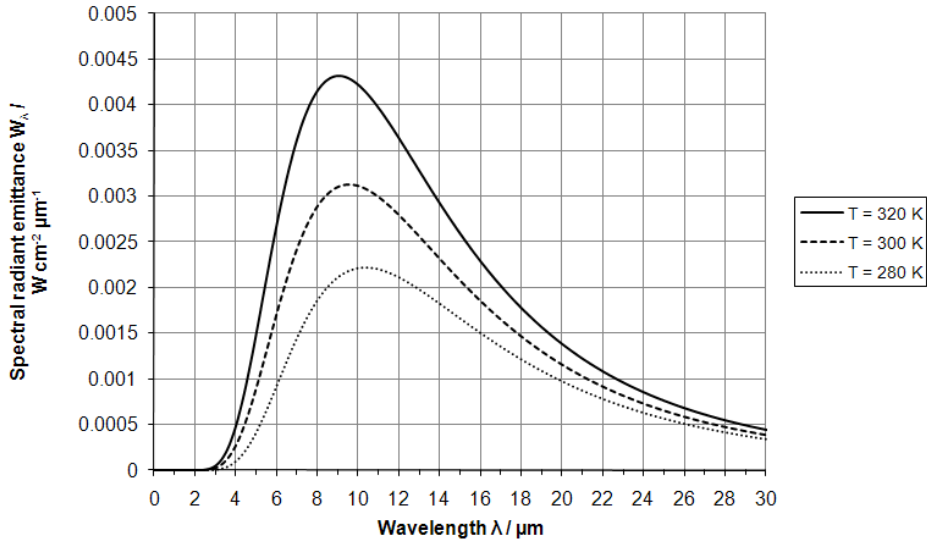


Figure 2.4: Spectral radiant emittance W_{λ} of 'Black body' at temperatures between $280 K \leq T \leq 320 K$

Wavelengths λ_m at maximum spectral radiant emittance for absolute temperatures T in Figure 2.4, calculated with Wien's displacement law are:

$$\lambda_m(280 K) = \frac{2897.8 \mu m K}{280 K} = 10.34 \mu m \quad (2.13)$$

$$\lambda_m(300 K) = \frac{2897.8 \mu m K}{300 K} = 9.66 \mu m \quad (2.14)$$

$$\lambda_m(320 K) = \frac{2897.8 \mu m K}{320 K} = 9.1 \mu m \quad (2.15)$$

The human body temperature is about $T_{\circ C} = 37 \text{ }^{\circ}C$ [6]. The human skin regulates the body temperature and varies its own temperature. Its temperature is approximately $T = 33 \text{ }^{\circ}C =$

2 Thermal radiation

306.1 K if the person stays in a room at room temperature. A 'Black body' with a temperature of $T_K = 306.1 K$ has its maximum spectral radiant emittance at a wavelength of $\lambda_m = 9.5 \mu m$.

$$\lambda_m(306.1 K) = \frac{2897.8 \mu m K}{306.1 K} = 9.5 \mu m \quad (2.16)$$

According to Figure 2.4 and reference [7] human skin has its highest spectral radiant emittance W_λ in the wavelength range

$$8 \mu m < \lambda < 14 \mu m. \quad (2.17)$$

To detect a person this infrared wavelength region should be used. Most of the human body is covered with cloths. This influences the infrared radiation emitted by human skin. Cloths emit, transmit and reflect radiation depending on the material.

3 Detectors for infrared radiation

Principally there are two possibilities to detect infrared radiation. First is with thermal detectors, second with photo or quantum detectors. Photo detectors transfer the energy of an incident photon to an electron in the detector material. This effect is called photo effect with a very short response time [8]. Thermal detectors have larger response times which are sufficient for this application.

3.1 Thermal detectors

Incident radiation causes a heating effect which changes some physical properties of the detector. The response time is typically a few milliseconds or longer [8]. This is adequate for human detection application. The majority of these detectors don't require cooling and found universal acceptance in a wide field of applications. Thermal detectors respond theoretically to all wavelengths, however in practice there are limitations and it is not necessary to detect any wavelength, rather it is necessary to detect a certain wavelength range. Currently there are a lot of different thermal detectors on the market. Thermocouples consist of a junction between two different metals such as nickel and constantan and produce a temperature related output voltage. Bolometers change their resistance when incident radiation heats the material. Pyroelectrics react on change in temperature with change in electric charge. Pyroelectric sensors are mostly manufactured from single crystals. This makes them cost effective and they don't need any additional power supply. This document is based on pyroelectric infrared detection to detect the emitted human infrared radiation.

3.2 The pyroelectric effect

Pyroelectric materials react on change in temperature with change in charge at the surface. This change in charge can be amplified and provided as a voltage or current output.

The surface charge of a pyroelectric crystal is usually neutralized by free carriers. Incident radiation with modulated frequency will be absorbed by the blackened surface. This absorp-

tion causes a temperature change of the material with the same frequency as the modulation frequency from the incident radiation. This temperature change alters the lattice spacing of the material and produces a change in spontaneous polarization. This produces an electrical current to balance the polarization change and causes a release of electric charge at the surface of the material.

This effect occurs only in polar, single crystals. These include ceramics or polymers like lithium tantalate ($LiTaO_3$) or sodium nitrite ($NaNO_2$). The pyroelectric materials are characterised by different properties like the pyroelectric coefficient p , shown in Table 3.1 for different materials.

Material	$p / \frac{\mu C}{m^2 K}$
$LiTaO_3$, single crystal	230
Lead zirconate titanate (PZT)	400
Triglycine sulfate (TGS), single crystal	280
Strontium barium niobate (SBN-50), single crystal	550
PbTiO ₃ , ceramic	180

Table 3.1: Pyroelectric coefficient p of some materials [9] [10]

The secondary pyroelectric effect is based on the piezoelectric effect. When pressure is applied to the crystals, an electric charge appears across the material. This pressure can be applied through thermal expansion or, for example, via mechanical stress. Therefore pyroelectric materials are very sensitive against mechanical stress.

The basic design of an electroded pyroelectric element is shown in Figure 3.1.

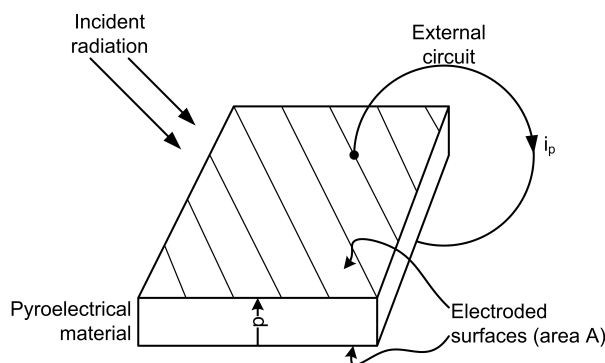


Figure 3.1: Pyroelectric element with electrodes while change in temperature [11]

The electroded surface has an area A . A change in temperature ΔT causes a change in charge ΔQ in the time Δt as shown in the Equation 3.1.

$$i_p = \frac{\Delta Q}{\Delta t} = \frac{A \cdot p \cdot \Delta T}{\Delta t}. \quad (3.1)$$

This report bases on a pyroelectric sensor which uses a lithium tantalite ($LiTaO_3$) single crystal sensor element. This sensor has a high performance and a wide availability.

3.3 Pyroelectric detectors

To detect a person with a pyroelectric detector the thermal emission from a person must be different from that of the background. This occurs if the skin temperature is different to the background temperature. Difficulties may occur if the background temperature and the skin temperature are nearly equal.

Various manufacturers offer different types of pyroelectric infrared detectors which are based on the technology explained in section 3.2. The typical conversion stages from pyroelectric infrared detectors are shown in Figure 3.2. The incident radiation flux ϕ_s pass an infrared filter with a transmission rate τ_F . The pyroelectric element absorbs the passed flux ϕ_s and causes a change in temperature ΔT_p in the element. The thermal to electrical conversion is due the pyroelectric effect, explained in section 3.2, which reacts on a change in temperature ΔT_p with a change in charge ΔQ_p . An external or internal circuit provides the electrical conversion from change in charge ΔQ_p into change in voltage Δu_s or change in current Δi_s [12].

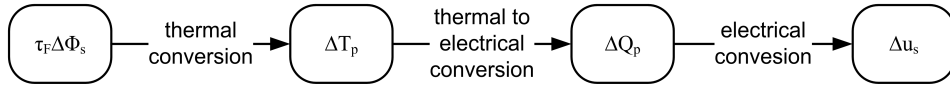


Figure 3.2: Conversion stages of the pyroelectric infrared detector [12]

3.3.1 Thermal conversion

In Figure 3.3 is the simplified thermal model of pyroelectric detectors, which converts the incident flux $\Delta \phi_s$ into a temperature change ΔT_p . Figure 3.4 depicts the same conversion in an equivalent electrical circuit. A pyroelectric material is characterised by the absorption rate α , the heat capacity H_p and the thermal conductance G_T to its surroundings. The surroundings are represented by a heat sink with a temperature T_A .

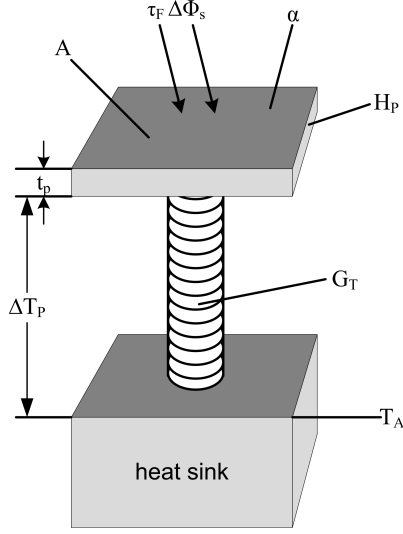


Figure 3.3: Simplified thermal model from a pyroelectric detector [12]

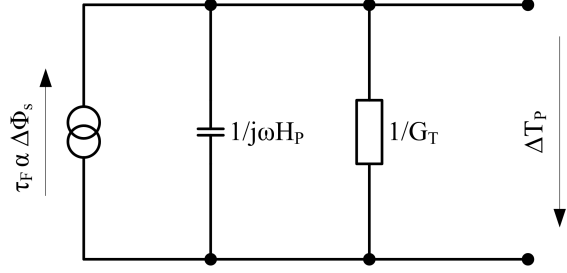


Figure 3.4: Electrical circuit from the simplified thermal model of the pyroelectric detector [12]

The heat capacity H_p and the thermal conductance G_T give the thermal time constant τ_T .

$$\tau_T = \frac{H_P}{G_T} \quad (3.2)$$

The temperature change ΔT_p is explained with the Equation 3.3 [12].

$$\Delta T_p = \frac{\alpha \cdot \tau_F \cdot \Delta \phi_s}{\sqrt{G_T^2 + \omega \cdot H_P^2}} \quad (3.3)$$

To detect small flux changes $\Delta \phi_s$ the product $\alpha \cdot \tau_F$ has to be near 100%. This can be achieved with the use of an absorption layer to get a high absorption α .

For small thermal time constants τ_T the heat capacity value H_P has to be low which can be achieved with small thickness t_p of the pyroelectric element.

3.3.2 Thermal to electrical conversion

The thermal to electrical conversion is due to the pyroelectric effect and is proportional to the detector's surface area A and the temperature change ΔT_p as explained in section 3.2. The output current i_p from the pyroelectric element follows the Equation 3.1 on page 22.

3.3.3 Electrical conversion

To convert the current i_p into an output signal to supply the next electrical circuit it is necessary to amplify it. This amplification can be done with a current or a voltage follower. Manufacturers often offer their pyroelectric detectors in a package with a first amplification stage included to prevent noise.

The two basic pre-amplifier circuits realised with operation amplifiers are the voltage and the current follower. These are shown in Figure 3.5 and Figure 3.6.

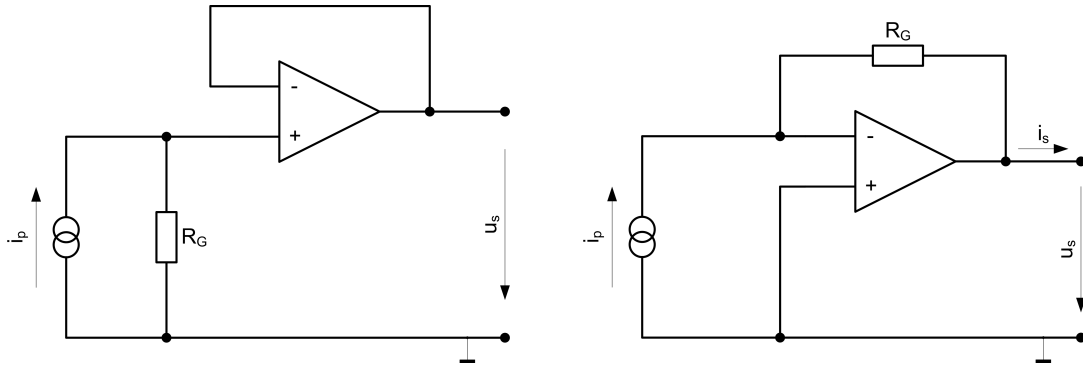


Figure 3.5: Voltage follower realized with an ideal operational amplifier
 Figure 3.6: Current follower realized with an ideal operational amplifier

The voltage follower in Figure 3.5 has an amplification of $u_s = R_G \cdot i_p$ and the current follower in Figure 3.6 has an amplification of $i_s = -R_G \cdot i_p$. Both circuits have high input impedance and low output impedance. In conclusion they don't load the sensing element and offer a low impedance output to supply the next amplification stage. Most of the manufacturers use for the first amplification one FET transistor as a voltage follower.

3.3.4 Compensation

Each pyroelectric material reacts to mechanical stress with change in charge. This produces an unwanted electrical output signal. To reduce the reaction of a sensor to mechanical stress like vibration it is necessary to compensate the element. The compensation can be done as a parallel compensation like shown in Figure 3.7. The sensor in Figure 3.7 is a dual element detector with two sensing elements. The sensing elements are parallel compensated. If both are exposed to the same mechanical stress the compensation eliminates the unwanted signal. Only one sensing element reacts on the incident radiation, the other element is isolated and doesn't receive any radiation. The followed amplification is realised with a FET voltage follower. Furthermore to compensate the sensing element the serial compensation is also possible.

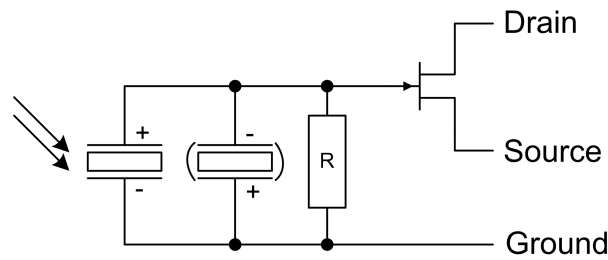


Figure 3.7: Compensation of the pyroelectric sensing element with a second pyroelectric sensing element. They are oppositely connected and one of them is isolated against incident radiation [13].

3.4 Optical system

This section describes the optical system between the sensing element and the radiation source. The radiation source is a person and the sensing element is a pyroelectric detector. A lens focuses the incident radiation, emitted by the person, on the detector. This lens increases the power of the radiation which is detected from the sensing element, because the area from the lens is bigger than the area from the sensing element.

3.4.1 Fresnel lens for incident radiation

A lot of different lenses for different applications exist on the market. They are defined by the focal length, size, material, etc.. Depending on the material the transmittance τ at different wavelengths λ varies. For this application a lens with high transmittance τ in the infrared region is required. Materials which have a high transmission τ in the infrared region are crystalline quartz (SiO_2), calcium fluoride (CaF_2), germanium (Ge) [8] or polymers like polyethylene based materials.

To make the lens smaller and cheaper the material must be reduced. This can be achieved with a Fresnel lens which is shown in Figure 3.8. Any point on a Fresnel lens has the same angle of incidence as the equivalent point on a convex lens. The transmittance τ from a Fresnel lens compared with a normal lens of the same material is higher because of the thinner lens.

3.4.2 Relation between the person and the sensor output frequency

To focus the emitted infrared radiation from the person on the sensing element the lens has to be positioned that the focal point from it is focused on the sensing element.

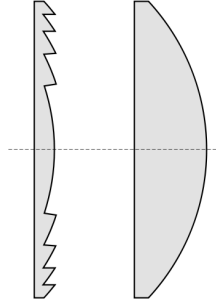


Figure 3.8: Graphic example for a Fresnel lens on the left and a normal lens on the right. Both have the same focal length [14]

This is archived if the distance between the sensing element and the lens is equivalent to the focal length f_b . The focal length f_b is a lens parameter.

The electric output signal from the sensing element can be described with its frequency f_{sens} . Knowledge about the output frequency range is important to design an amplifier circuit.

The output frequency f_{sens} from the sensing element depends on the working distance L and the walking velocity v_b from the person. The working distance L is the distance between the lens and the person. Figure 3.9 shows the application with a person, a lens and the sensing element. The sensing element has the size s .

The Equation 3.4 describes the relation between the focal length f_b , the velocity v_b , the sensing element size s , the working distance L and the sensor output frequency f_{sens} .

$$f_{sens} = \frac{v_b \cdot f_b}{2\pi \cdot s \cdot L} \quad [15] \quad (3.4)$$

where

f_b = focal length, m

f_{sens} = frequency, Hz

v_b = velocity, walking speed, $\frac{m}{s}$

s = size of sensing element, m

L = working distance, m

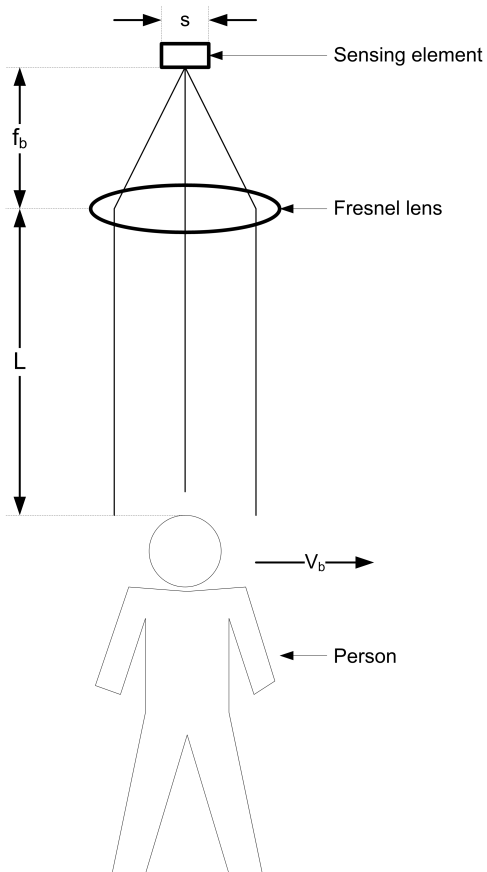


Figure 3.9: Optical system between the person and the sensing element with a Fresnel lens. Variables: Walking velocity v_b , output frequency f_{sens} , sensing element size s , focal length f_b .

4 Electrical Filters

This chapter describes the basics about analogue electrical filters. A high pass filter and two non inverted band pass filters are used for the sensor board schematic in subsection 5.1.3.

4.1 High pass filter

A high pass filter is used in the sensor board schematic in subsection 5.1.3 to eliminate a DC offset voltage. A high pass filter can be build with passive components, like a resistor and a capacitor. A high pass filter with one resistor and one capacitor is shown in Figure 4.1.

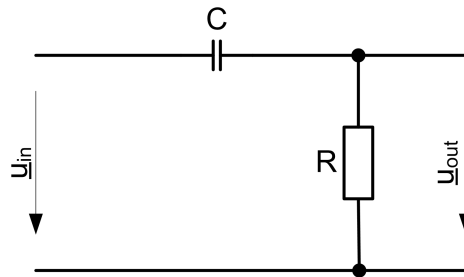


Figure 4.1: High pass filter with the passive components resistor R and capacitor C

With passive components it is not possible to filter and amplify the signal with a gain $|v| > 0 \text{ dB}$. To archive an amplification $|v| > 0 \text{ dB}$ it is necessary to use active components like operational amplifiers. The transfer function from the high pass filter in Figure 4.1 with resistor R and capacitor C is

$$\underline{v} = \frac{U_{out}}{U_{in}} = \frac{R}{\frac{1}{j\omega C} + R} = \frac{1}{\frac{1}{j\omega RC} + 1} = \frac{1}{\frac{1}{j2\pi fRC} + 1}. \quad (4.1)$$

The 3 dB cut off frequency f_c of this high pass filter can be calculated with

$$f_c = \frac{1}{2\pi RC}. \quad (4.2)$$

The amplitude response $|v|$ and the 3 dB cut off frequency f_c from a high pass filter with $C = 47 \mu\text{F}$ and $R = 1 \text{ M}\Omega$ is shown in Figure 4.2.

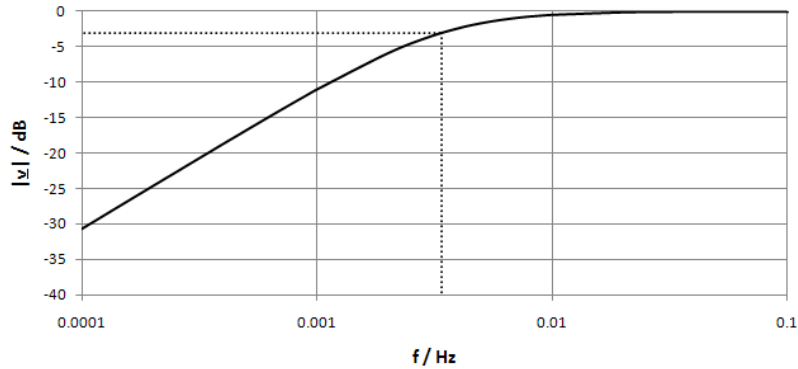


Figure 4.2: Amplitude transfer function versus frequency for a high pass filter with $C = 47 \mu F$ and $R = 1 M\Omega$. The dotted line represents the 3 dB cut off frequency f_c

The output and input impedance from this high pass filter with passive components depends on the electrical components before and the electrical components after the filter. This filter doesn't work as an impedance converter because input and output are connected through R and C .

4.2 Band pass filter

This section provides basics about inverted and non inverted band pass filters with operational amplifiers. Two non inverted band pass filters are used for the sensor board schematic in subsection 5.1.3.

4.2.1 Inverted band pass filter

Figure 4.3 shows an inverted amplifier circuit realised with one operational amplifier. The filter characteristics from this amplifier circuit depends on the values from \underline{Z}_1 and \underline{Z}_2 . This amplifier circuit in Figure 4.3 has the transfer function

$$\underline{v} = \frac{U_{out}}{U_{in}} = -\frac{\underline{Z}_1}{\underline{Z}_2}. \quad (4.3)$$

Discretising \underline{Z}_1 with an RC parallel component and \underline{Z}_2 with an RC serial component the amplifier becomes a band pass filter with amplification. \underline{Z}_1 defines the upper cut off frequency f_h and \underline{Z}_2 the lower cut off frequency f_l . Figure 4.4 shows this band pass filter with discrete components.

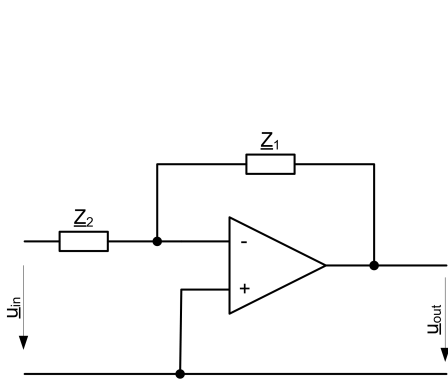


Figure 4.3: Inverted amplifier circuit with an operational amplifier and external components

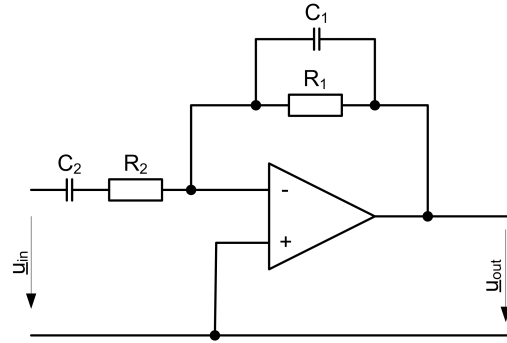


Figure 4.4: An operational amplifier with discrete components. The circuit acts as a inverted band pass filter with amplification

The input impedance z_{in} which is seen by the source connected to \underline{U}_{in} can be calculated with the virtual null point from the operational amplifier.

$$z_{in} = \frac{u_{in}}{i(Z_2)} = \frac{u_{in}}{u_{in}Z_2} = \underline{Z}_2 \quad (4.4)$$

The input impedance z_{in} is not infinite and depends on \underline{Z}_2 of the band pass filter circuit. The transfer function \underline{v} from the inverted band pass filter with amplification in Figure 4.4 is described with

$$\underline{v} = \frac{u_{out}}{u_{in}} = -\frac{1}{\frac{j\omega C_1 + \frac{1}{R_1}}{\frac{1}{j\omega C_2} + R_2}}. \quad (4.5)$$

4.2.2 Non inverted band pass filter

Two non inverted band pass filters are used for the sensor board schematic in subsection 5.1.3. Figure 4.5 shows a non inverted amplifier circuit realised with an operational amplifier and external components. The filter characteristics from this amplifier circuit depends on the values from \underline{Z}_1 and \underline{Z}_2 and has the transfer function

$$\underline{v} = \frac{U_{out}}{U_{in}} = 1 + \frac{Z_1}{Z_2} \quad (4.6)$$

Discretizing \underline{Z}_1 with an RC parallel component and \underline{Z}_2 with an RC serial component the non inverted amplifier circuit becomes a non inverted band pass filter. \underline{Z}_1 defines the upper cut off frequency f_h and \underline{Z}_2 the lower cut off frequency f_l . Figure 4.6 shows the non inverted band pass filter with discrete components.

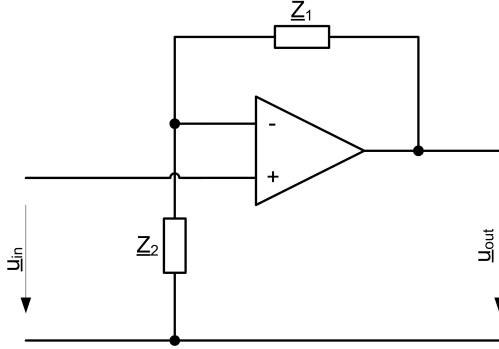


Figure 4.5: Non inverted amplifier circuit with an operational amplifier and external components

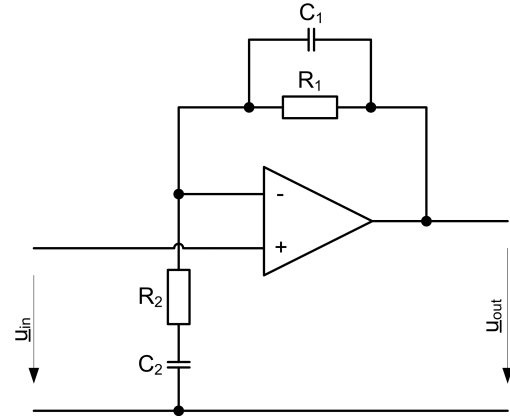


Figure 4.6: An operational amplifier with discrete components. The circuit acts as a non inverted band pass filter with amplification

The input impedance z_{in} which is seen by the source connected to U_{in} can be calculated as followed

$$z_{in} \approx \frac{u_{in}}{i_{in}} \underset{i_{in} \rightarrow 0}{=} \infty. \quad (4.7)$$

The input impedance z_{in} is infinite and doesn't depend on the external components from the operational amplifier. The transfer function \underline{v} of the inverted band pass filter is described like

$$\underline{v} = \frac{U_{out}}{U_{in}} = 1 + \frac{\frac{1}{j\omega C_1 + \frac{1}{R_1}}}{\frac{1}{j\omega C_2} + R_2} \quad (4.8)$$

with upper cut off frequency

$$f_h = \frac{1}{2\pi R_1 C_1}, \quad (4.9)$$

lower cut off frequency

$$f_l = \frac{1}{2\pi R_2 C_2}, \quad (4.10)$$

middle frequency

$$f_0 = \frac{f_h + f_l}{2}, \quad (4.11)$$

and bandwidth

$$b = f_h - f_l. \quad (4.12)$$

The gain at middle frequency f_0 is

$$v_{f_0} = 1 + \frac{R_1}{R_2}. \quad (4.13)$$

Figure 4.7 shows the amplitude transfer function versus frequency for a non inverted band pass filter with gain at middle frequency $v_{f_0} = 27 \text{ dB}$, upper cut off frequency $f_h = 10.6 \text{ Hz}$ and lower cut off frequency $f_l = 72 \text{ mHz}$.

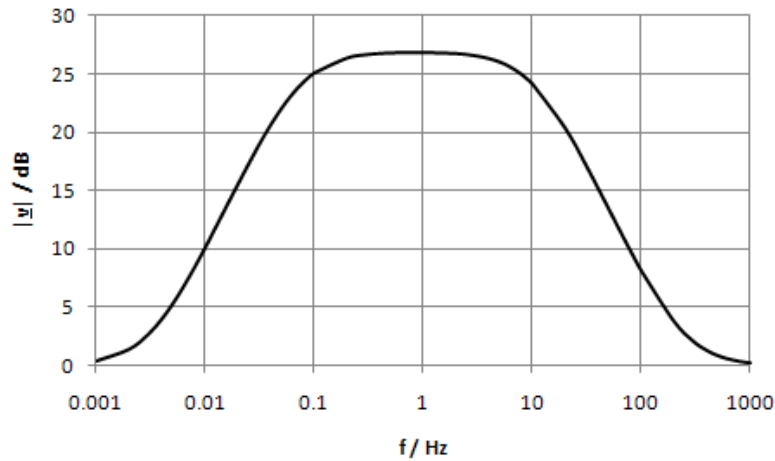


Figure 4.7: Amplitude transfer function versus frequency for a non inverted band-pass filter with an ideal operational amplifier and discrete components

Band pass filter $BP1$ in the sensor board schematic in subsection 5.1.3 has the same values for the gain at middle frequency v_{f_0} , upper cut off frequency f_h and lower cut off frequency f_l .

5 Proposed design

This chapter explains the proposed experimental kit which monitors an area with four infrared detectors. The experimental kit should be able to plot the output signals from four infrared detectors in a Windows environment. The proposed experimental kit consists of three units. The first unit is a sensor box which is described in the section 5.1. The sensor box consists of a lens, the sensor and an electrical filter and amplifier circuit. The second unit is a microcontroller which is described in the section 5.2. The microcontroller digitises the analogue sensor box output signals and sends them via the serial port to the computer. The third unit is the software for the computer which is described in the section 5.3. Figure 5.1 shows the interaction between the infrared radiation emitted by a human and the software on a personal computer.

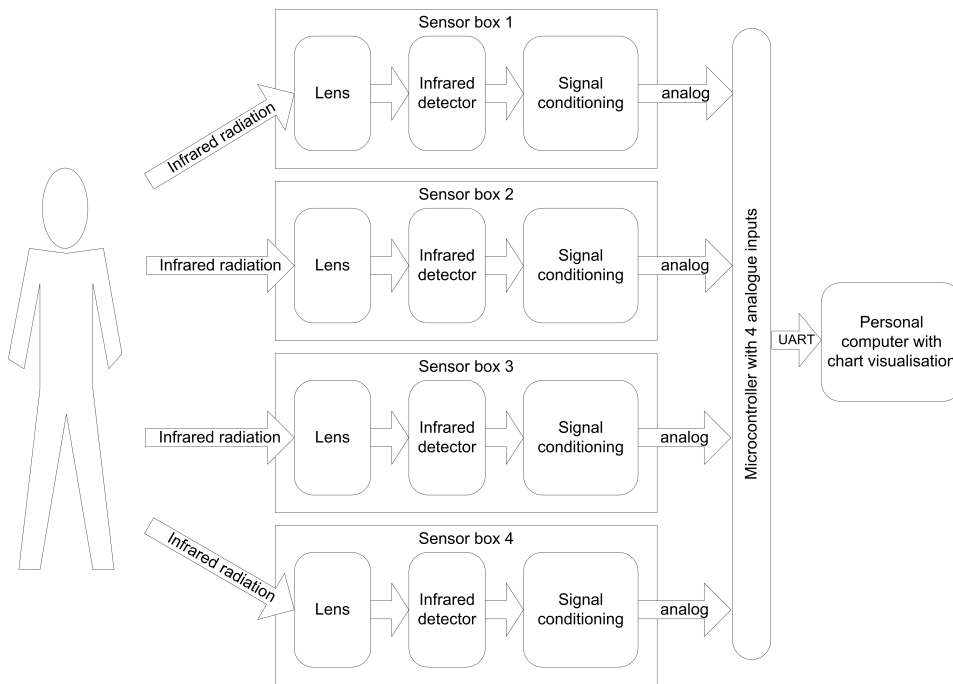


Figure 5.1: Flow chart from the proposed experimental kit. A person emits infrared radiation. This radiation is detected with four sensor boxes. The computer software plots the output signal from the sensor boxes in a chart.

5.1 Capture of signal data

This section describes the sensor box which consists of the sensor board and a lens. The sensor board is made of an infrared sensor and an electronic circuit to filter and amplify the signal.

5.1.1 Fresnel lens

To focus the incident infrared radiation on the infrared detector a Fresnel lens, like explained in Subsection 3.4.1 on page 25 is used. Fresnel Technologies Inc. is a manufacturer of Fresnel lenses and offers a wide range of them. They offer the three different materials POLY IR 2, 4 and 7 for the wavelength between $8 \mu m$ and $14 \mu m$. This range is used for the human detection as mentioned in section 2.5 on page 18. POLY IR 2, 4 and 7 are material names from Fresnel Technologies Inc. and polyethylene based. This material is cheaper and easier to manufacture than, for example, germanium. POLY IR 7 is not ultraviolet stabilized and therefore not for the use with sunlight. POLY IR 2 and 4 are both ultraviolet stabilized. Poly IR 2 has the least absorption loss in the $8 \mu m$ to $14 \mu m$ region. In conclusion the Poly IR 2 material is chosen for the used Fresnel lens. The transmittance τ of POLY IR 2 is shown in Figure 5.2.

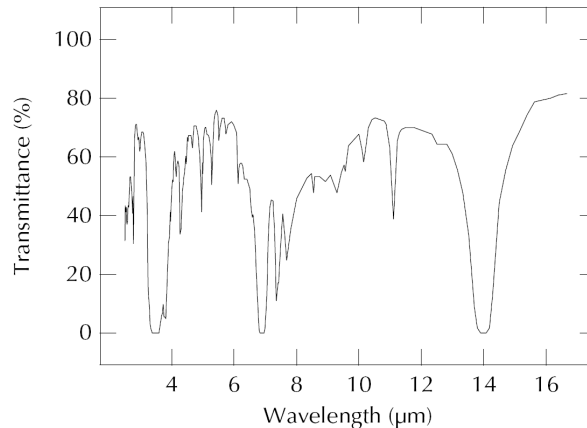


Figure 5.2: Transmittance τ of POLY IR 2 material as a function of the wavelength λ . Thickness = 0.38 mm [7]

The focal length f_b and the overall size of the Fresnel lens is important because the sensor box should be as small as possible. Therefore the smallest Fresnel lens from Fresnel Technologies Inc. is used which has a focal length of $f_b = 4.5 \text{ mm}$ and an overall size of $15 \cdot 15 \text{ mm}$.

5.1.2 Dual Element Detector LHi 958

The Dual Element Detector LHi 958 from PerkinElmer is available at the Edinburgh Napier University. It consists of two sensing elements to compensate noise as mentioned in subsection 3.3.4 on page 24 . The sensor has two oppositely connected sensing elements to provide a different output signal depending on the moving direction of the person. Figure 5.3 shows a sensor output signal.

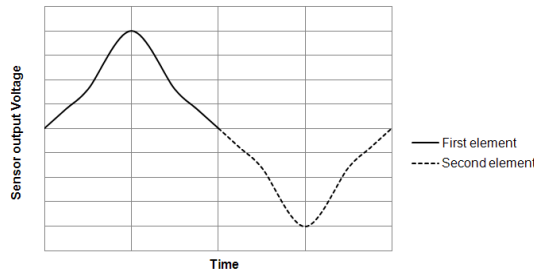


Figure 5.3: Sensor output signal generated by a person moving from the left to the right [15]

If the person moves from the left to the right the first sensing element provides the first part of the output signal and the second sensing element provides the second part of the output signal. If the person moves from the right to the left the second sensing element provides the first part of the output signal and the first sensing element provides the second part of the output signal.

The Dual Element Detector LHi 958 has one voltage follower and an optical filter as shown in Figure 5.4.

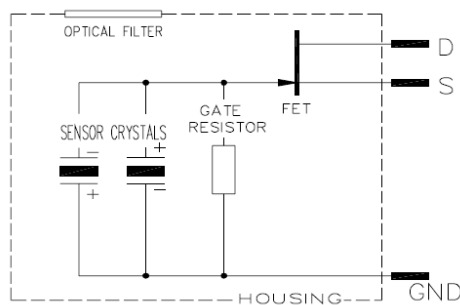


Figure 5.4: Dual element detector LHi 958 [13]

The substrate of the optical filter is multilayer coated silicon. This material has a transmission τ about $\tau = 77\%$ for a wavelength between $\lambda = 7\mu m$ and $\lambda = 14\mu m$. This wavelength

5 Proposed design

range includes the standard range for human detection which is calculated in Equation 2.17 on page 19. The two separate lithium tantalite ($LiTaO_3$) crystal sensing elements are connected to a voltage (source) follower. Lithium tantalite is a pyroelectric material with the pyroelectric coefficient $p = 230 \frac{\mu C}{m^2 K}$ as shown in Table 3.1 on page 21.

The operating voltage is between 2 V and 15 V and the offset output voltage between 0.2 V and 1.5 V. All values are referenced to an output resistance of $R_s = 47 k\Omega$ [13].

The dual element detector has an element size $s = 1 mm$. The working distance L between the detector and the person is approximately between $1 m < L < 4 m$. The walking speed v_b from the person vary between $0.8 \frac{m}{s}$ if the person walks very slow and $5.5 \frac{m}{s}$ if the person runs. Equation 3.4 on page 26 gives the extreme values for the dual element detector output frequency. This frequency range must be amplified and filtered from the electronic circuit after the detector.

The dual element detector output frequency f_{sens} is between 143 mHz and 3.9 Hz.

$$f_{sens_{min}} \approx \frac{0.8 \frac{m}{s} \cdot 4.5 mm}{2\pi \cdot 1 mm \cdot 4 m} = 143 mHz \quad (5.1)$$

$$f_{sens_{max}} \approx \frac{5.5 \frac{m}{s} \cdot 4.5 mm}{2\pi \cdot 1 mm \cdot 1 m} = 3.9 Hz \quad (5.2)$$

The frequency responsivity of the dual element detector LHi 958 is shown in Figure 5.5. At a frequency of $f = 143 mHz$ the responsivity is about $R = 10 \frac{kV}{W}$ and for a frequency of $f = 3.9 Hz$ the responsivity is about $R = 0.9 \frac{kV}{W}$. That means that output signal is higher for lower input frequencies and lower for higher input frequencies.

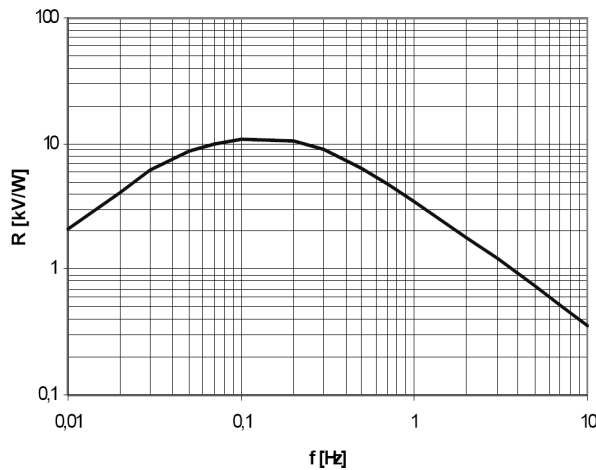


Figure 5.5: Responsivity versus frequency from dual element detector LHi 958 [13]

5.1.3 Sensor board schematic

This subsection describes the sensor board development which includes the infrared detector and the electronic circuit. This circuit filters and amplifies the detectors output signal. Figure 5.6 shows the signal flow from the sensor output V_{in} to the board output V_{out} .

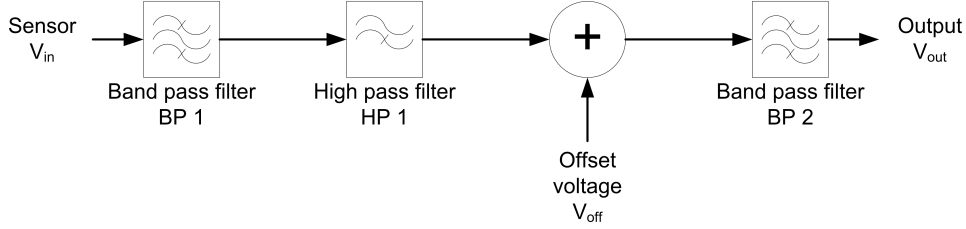


Figure 5.6: Signal flow chart for board schematic

The sensor output signal $V_{in} = V_{in\ off} + V_{in\ sig}$ where $V_{in\ off}$ is the sensor output offset voltage and $V_{in\ sig}$ is the sensor output signal. The signal $V_{in\ sig}$ should be conditioned and provided as the sensor board output voltage $V_{out} = V_{out\ off} + V_{out\ sig}$ where $V_{out\ off}$ is the sensor board output offset voltage and $V_{out\ sig}$ is the filtered and amplified sensor signal $V_{in\ sig}$. Most microcontrollers have an analogue input range between $0\ V$ and $2.5\ V$. The board output signal V_{out} should be in this voltage range. In conclusion the board output offset voltage is $V_{out\ off} = 1.25\ V$

$$V_{out\ off} = \frac{2.5\ V}{2} = 1.25\ V \quad (5.3)$$

The output signal amplitude $\widehat{V}_{out\ sig}$ should not exceed $1.25\ V$.

For a maximum board output voltage of $V_{out} = 2.5\ V$ it is sufficient to supply the circuit with $3.3\ V$. Supplying the dual element detector LHi 958 with this voltage the sensor output offset voltage $V_{in\ off}$ is approximately $800\ mV$. The first test by moving a hand over the sensor provided an output signal amplitude $\widehat{V}_{in\ sig}$ of approximately $10\ mV$. This sensor output signal $\widehat{V}_{in\ sig} = 10\ mV$ has to be amplified to a board output signal $\widehat{V}_{out\ sig} = 1.25\ V$. Therefore the amplification v_{f0} of the sensor board should be maximal $v_{f0\ max} = 125$.

$$v_{f0\ max} = \frac{\widehat{V}_{out\ sig}}{\widehat{V}_{in\ sig}} = \frac{1.25\ V}{10\ mV} = 125 \quad (5.4)$$

The sensor output signal $V_{in\ sig}$ has to be amplified in a frequency range between $143\ mHz$ and $3.9\ Hz$ as calculated in the Equation 5.1 and Equation 5.2 on page 36. This can be realised with band pass filters.

To amplify the signal with an inverting filter the circuit needs a dual supply voltage. For

5 Proposed design

this reason to amplify and filter the sensor output signal V_{in} a non inverting band pass filter $BP1$ is used. This band pass filter $BP1$ has a very high input impedance so that it doesn't load the sensor and a minimum gain of 0 dB over all frequencies. The gain at middle frequency from this band pass filter can not be higher than $v_{f0max}(BP1) = 80$.

$$v_{f0max}(BP1) = \frac{V_{in\ off}}{\widehat{V}_{in\ sig}} = \frac{800\ mV}{10\ mV} = 80 \quad (5.5)$$

This is due to the voltage range, predetermined by the offset voltage $V_{in\ off}$, is not enough to amplify the signal with a higher gain. In conclusion a second band pass filter with a higher offset voltage V_{off} amplifies and filters the signal again.

After the band pass filter $BP1$ the high pass filter $HP1$ cuts the DC offset $V_{in\ off}$ and adds the new offset voltage V_{off} . This signal is filtered and amplified with the second band pass filter $BP2$ which is also a non inverting filter to transmit the DC offset V_{off} with a gain of 0 dB . Noise with higher frequencies is attenuated.

The signal flow chart from Figure 5.6 is transformed into a schematic diagram. To build the sensor board the software Eagle 5.6.0 is used. The transformed schematic diagram is shown in Figure 5.7.

5 Proposed design

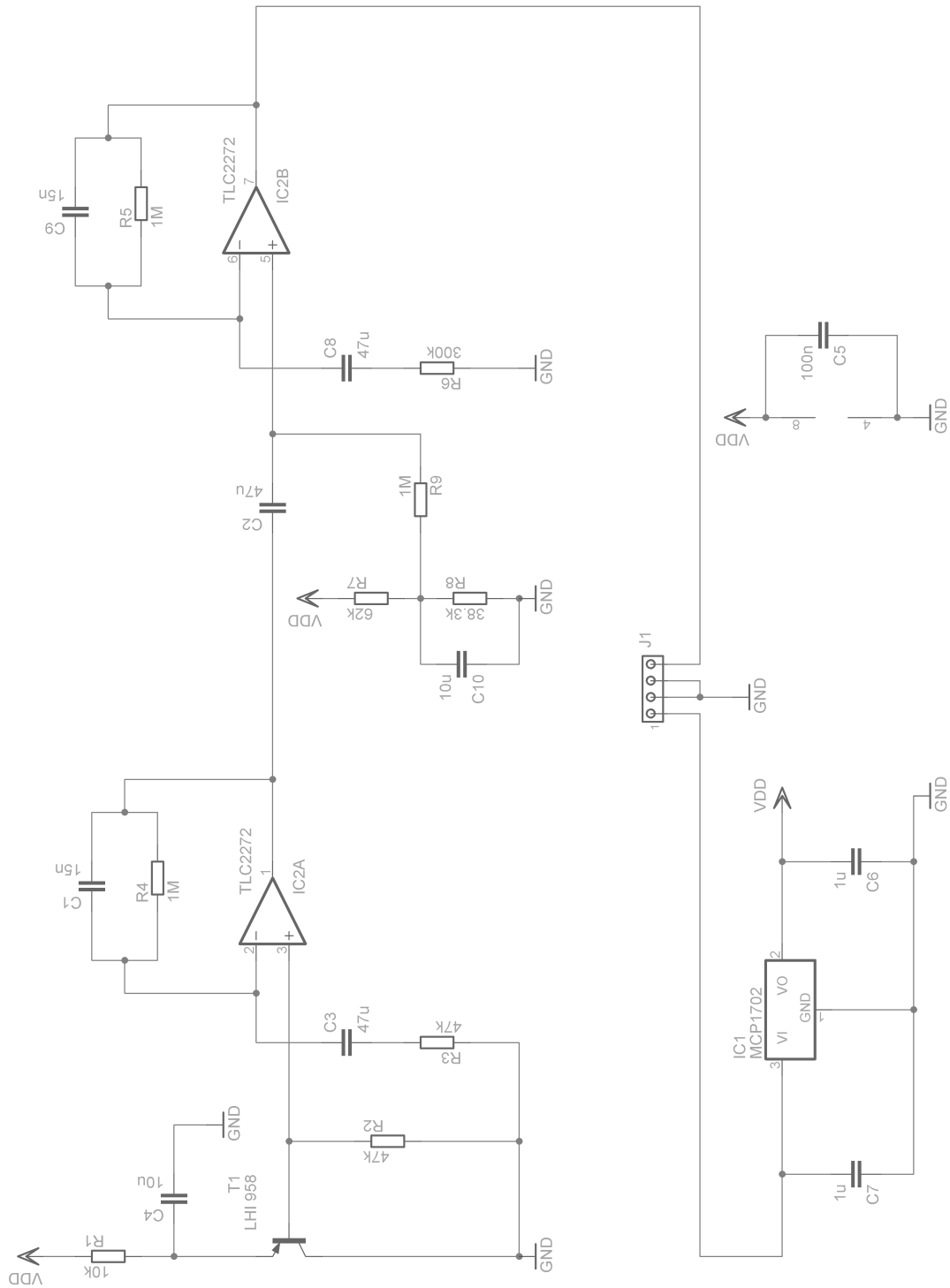


Figure 5.7: Schematic diagram of amplification and band pass Filter for infrared sensor LHi 958 in Eagle 5.6.0

5 Proposed design

Voltage regulator $IC1$ supplies together with $C6$ and $C7$ the board with $3.3 V$. $C5$ is the voltage stabilizing capacitor for $IC2$. Resistor $R1$ and Capacitor $C4$ build a low pass filter with a cut of frequency of $f_c = 1.59 Hz$.

$$f_{l(R_1, C_4)} = \frac{1}{2\pi R_1 C_4} = \frac{1}{2\pi \cdot 10 k\Omega \cdot 10 \mu F} = 1.59 Hz \quad (5.6)$$

This low pass filter supplies the dual element detector Lhi 958 $T1$ with a filtered DC voltage. The load Resistor $R2$ is recommended with a value $R_2 = 47 k\Omega$ from the detector manufacturer [13]. The detector output signal $TP3$ becomes filtered by the band pass filter $BP1$ with operational amplifier $IC2A$ with the following transmission characteristic:

Transmission function v_{BP1} :

$$v_{BP1} = 1 + \frac{\frac{1}{j\omega C_1 + \frac{1}{R_4}}}{\frac{1}{j\omega C_3} + R_3} = 1 + \frac{\frac{1}{j \cdot 2\pi \cdot f \cdot 15 nF + \frac{1}{1 M\Omega}}}{\frac{1}{j \cdot 2\pi \cdot f \cdot 47 \mu F} + 47 k\Omega} \quad (5.7)$$

Upper cut off frequency f_h :

$$f_h = \frac{1}{2\pi R_4 C_1} = \frac{1}{2\pi \cdot 1 M\Omega \cdot 15 nF} = 10.6 Hz \quad (5.8)$$

Lower cut off frequency f_l :

$$f_l = \frac{1}{2\pi R_3 C_3} = \frac{1}{2\pi \cdot 47 k\Omega \cdot 47 \mu F} = 72 mHz \quad (5.9)$$

Middle frequency f_0 :

$$f_0 = \frac{f_h + f_l}{2} = \frac{10.6 Hz + 72 mHz}{2} = 5.34 Hz \quad (5.10)$$

Gain at middle frequency v_{f_0} :

$$v_{f_0} = 1 + \frac{R_4}{R_3} = 1 + \frac{1 M\Omega}{47 k\Omega} = 22.28 = 27 dB \quad (5.11)$$

After the first band pass filter $BP1$ a new DC offset from $1.25V$ must be added to the AC signal. Therefore high pass filter $HP1$ with capacitor $C2$ and resistor $R9$ with a cut off frequency $f_c = 3.39 mHz$ cuts the DC offset.

$$f_{c(R_9, C_2)} = \frac{1}{2\pi R_9 C_2} = \frac{1}{2\pi \cdot 1 M\Omega \cdot 47 \mu F} = 3.39 mHz \quad (5.12)$$

The transmission function from *HP1* is

$$\underline{v}_{HP1} = \frac{R_9}{\frac{1}{j\omega R_9 C_2} + 1}. \quad (5.13)$$

Furthermore with *R7*, *R8* and *R9* a new DC offset $V_{off} = 1.25 \text{ V}$ is added to the AC signal by *R9*.

$$V_{off} = V_{DD} \frac{R_8}{R_7 + R_8} = 3.3 \text{ V} \frac{38.2 \text{ k}\Omega}{62 \text{ k}\Omega + 38.2 \text{ k}\Omega} = 1.25 \text{ V} \quad (5.14)$$

After that the signal has to be band pass filtered and amplified (*BP2*) again. The lower cut off frequency f_l from band pass filter *BP2* is necessary to amplify the DC part of the signal with 0 dB and the higher cut of frequency f_h is necessary to reduce noise with a higher frequency than f_h . The second band pass filter *BP2* with operational amplifier *IC2B* has the following transmission characteristic:

Transmission function \underline{v}_{BP2} :

$$\underline{v}_{BP2} = 1 + \frac{\frac{1}{j\omega C_9 + \frac{1}{R_5}}}{\frac{1}{j\Omega C_8} + R_6} = 1 + \frac{\frac{1}{j \cdot 2\pi \cdot f \cdot 15 \text{ nF}} + \frac{1}{1 \text{ M}\Omega}}{\frac{1}{j \cdot 2\pi \cdot f \cdot 47 \text{ }\mu\text{F}} + 300 \text{ k}\Omega} \quad (5.15)$$

Upper cut off frequency f_h :

$$f_h = \frac{1}{2\pi R_5 C_6} = \frac{1}{2\pi \cdot 1 \text{ M}\Omega \cdot 15 \text{ nF}} = 10.6 \text{ Hz} \quad (5.16)$$

Lower cut off frequency f_l :

$$f_l = \frac{1}{2\pi R_6 C_8} = \frac{1}{2\pi \cdot 300 \text{ k}\Omega \cdot 47 \text{ }\mu\text{F}} = 11.3 \text{ mHz} \quad (5.17)$$

Middle frequency f_0 :

$$f_0 = \frac{f_h + f_l}{2} = \frac{10.6 \text{ Hz} + 11.3 \text{ mHz}}{2} = 5.31 \text{ Hz} \quad (5.18)$$

Gain at middle frequency v_{f_0} :

$$v_{f_0} = 1 + \frac{R_5}{R_6} = 1 + \frac{1 \text{ M}\Omega}{300 \text{ k}\Omega} = 4.33 = 12.7 \text{ dB} \quad (5.19)$$

To get the transmission characteristic of the entire circuit it is necessary to multiply the transmission functions from the band pass filter *BP1*, the high pass filter *HP1* and the band pass filter *BP2*. The transmission characteristic whose amplitude response is shown in Figure 5.8 and whose phase response in Figure 5.9 is simulated with Tina. Tina is software to simulate

analogue and digital electric circuits.

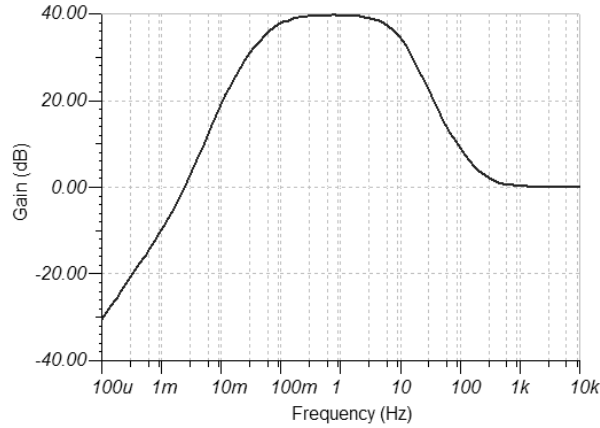


Figure 5.8: Amplitude response from board circuit simulated with Tina

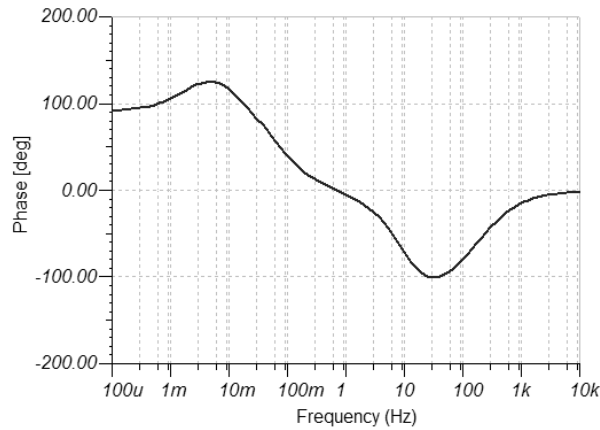


Figure 5.9: Phase response from board circuit simulated with Tina

Figure 5.10 shows an example for the board transmission of an input signal $V_{in} = V_{in\ off} + V_{in\ sig} = 800\ mV + 10\ mV \cdot \sin(2\pi \cdot 5\ Hz \cdot t)$ which represents the sensor output signal. Figure 5.10 is based on the schematic from Figure 5.7. $TP3$ in Figure 5.7 is the input signal V_{in} in Figure 5.10. The output signal at $pin\ 4$ on $J1$ in Figure 5.7 is represented by V_{out} in Figure 5.10.

The complete circuit has a transmission characteristic like a band pass filter with a very low amplification at lower frequencies and unity amplification at higher frequencies. The lower cut off frequency of the circuit is $f_l = 80\ mHz$ and the upper cut off frequency is $f_h = 7\ Hz$.

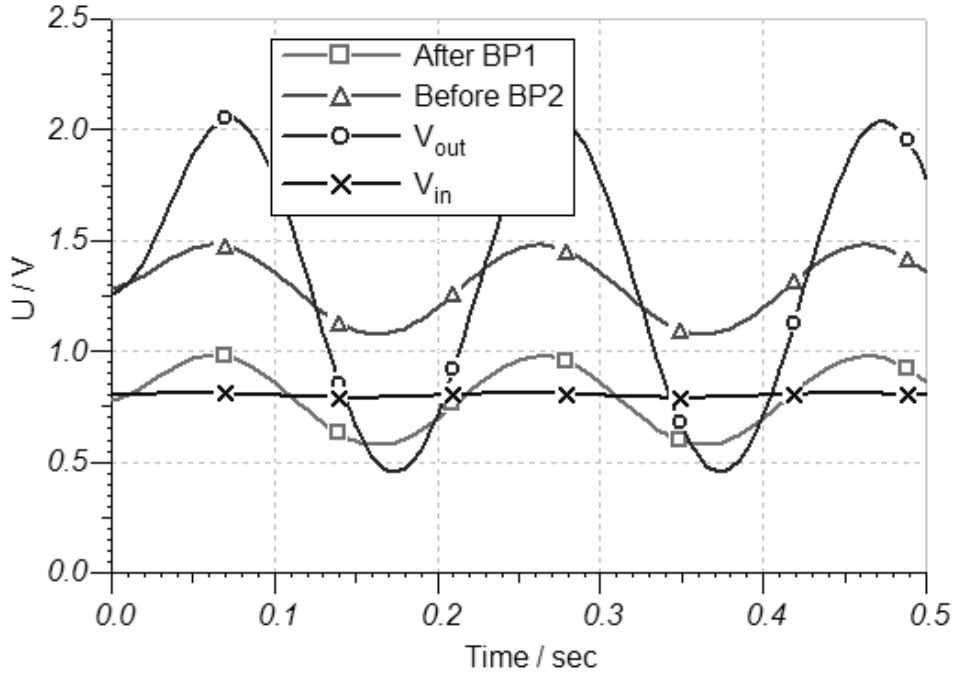


Figure 5.10: Time signal stages from board schematic with $V_{in} = 800 \text{ mV} + 10 \text{ mV} \cdot \sin(2\pi \cdot 5 \text{ Hz} \cdot t)$.

The calculated frequency range from the dual element detector LHi 958 in Equation 5.1 and Equation 5.2 on page 36 is between 143 mHz and 3.9 Hz . This frequency range can be amplified with this circuit.

From Equation 5.11 on page 40 and Equation 5.19 on page 41 follows that the gain at middle frequency from the sensor board is

$$v_{f_0(\text{sensor board})} = v_{f_0(\text{BP1})} + v_{f_0(\text{BP2})} = 27 \text{ dB} + 12.7 \text{ dB} = 39.7 \text{ dB} = 96.6. \quad (5.20)$$

The calculated maximal gain at middle frequency from the sensor board in Equation 5.4 on page 37 is $v_{f_0_{max}} = 125$. A gain at middle frequency from $v_{f_0(\text{sensor board})} = 96.6$ is therefore applicable for this application.

5.1.4 V0 sensor board layout

The sensor board schematic is transformed to a board layout with the software Eagle 5.6.0. Figure 5.7 shows the schematic which is transferred to the v0 board layout shown in Figure 5.11. The sensor board is populated by hand.

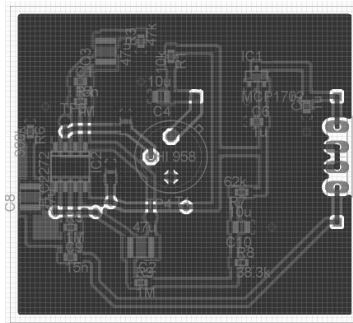


Figure 5.11: v0 sensor board layout for signal conditioning of infrared sensor LHi 958

Problems with the v0 sensor board layout were discovered while soldering the components. These are listed as followings:

- The available capacitor $C5 = 100 \text{ nF}$ at the University is larger than the proposed size 0603. It was possible to use a larger capacitor. For the next sensor board the capacitor $C5$ with size 0603 should be ordered.
- The space for $C2, C3, C8 = 47 \text{ }\mu\text{F}$ and $C4 = 10 \text{ }\mu\text{F}$ on the v0 sensor board layout is too small. It was possible to use other capacitors. For the next sensor board layout the space should be adapted to the size of the capacitors.
- The ground area on the top and on the bottom is through connected on a lot of points. One ground area on the bottom would be better for the next sensor board layout.
- Sensor LHi 958 should be rotated because the sensing elements are not parallel with the board exterior. This could cause complications for the use of the sensor box.

All errors mentioned in the error list could be solved with some simple redesigns and the v0 board layout could be produced. A photo of the top of the produced v0 sensor board is shown in Figure 5.12 and a photo of the bottom in Figure 5.13.

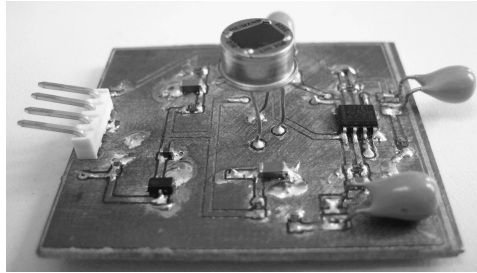


Figure 5.12: Photo from the top of the v0 sensor board

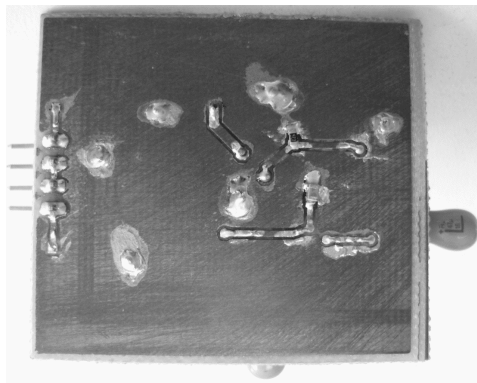


Figure 5.13: Photo from the bottom of the v0 sensor board

5.1.5 V0 sensor board hardware test

It is necessary to test the v0 sensor board to know if it works like expected. After connecting the sensor board to the power supply the amplitude transfer of the sensor board can be measured. The input of the v0 sensor board is the dual element infrared detector and the output is an electrical signal. To measure the amplitude transfer function an infrared signal at different frequencies is transmitted to the sensor board and an oscilloscope is used to measure the sensor board output signal. The Test assembly is shown in Figure 5.14.

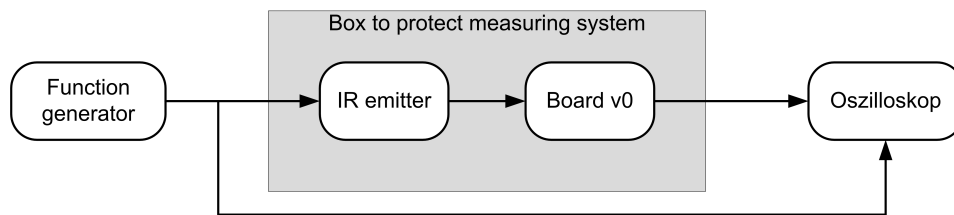


Figure 5.14: Test assembly for the hardware test for the sensor board

The function generator generates a voltage signal with variable frequency which is transmitted to the infrared emitter. The infrared emitter generates voltage proportional infrared radiation. This signal is emitted to the v0 sensor board. As it is a dual element sensor, one of the two sensing elements must be covered. If both of them would be exposed to the infrared radiation the output signal would be zero. To cover one sensing element a slit is used. The output signal from the v0 sensor board and the output signal from the function generator are captured by an oscilloscope which measures the amplitude transfer.

This measurement is very sensitive to thermal radiation. To protect the measuring system a shield is built around the IR emitter and the v0 board. A photo of the test assembly is shown in Figure 5.15.

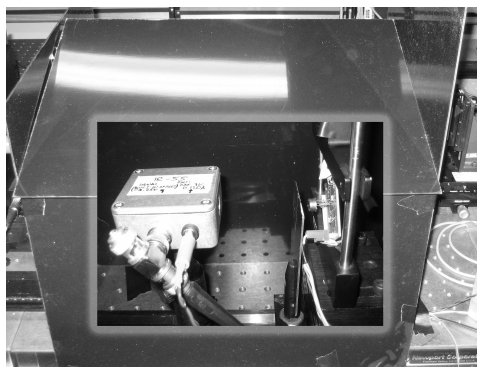


Figure 5.15: Photo from test assembly of the v0 board

The responsivity of the sensing element on the v0 sensor board is given by the sensor datasheet and shown in Figure 5.5 on page 36. The 'sensor responsivity' multiplied with the 'calculated filter and amplifier amplitude response' from the v0 sensor board gives the 'calculated sensor board amplitude response'. The 'calculated filter and amplifier amplitude response' is the amplitude response of the multiplication from the transmission function from *HP1*, *BP1* and *BP2*. The transmission function from *HP1* is given in Equation 5.13 on page 41, from *BP1* in Equation 5.7 on page 40 and from *BP2* in Equation 5.15 on page 41. The graphs 'sensor responsivity', 'calculated filter and amplifier amplitude response' and 'calculated sensor board amplitude response' are displayed in Figure 5.16.

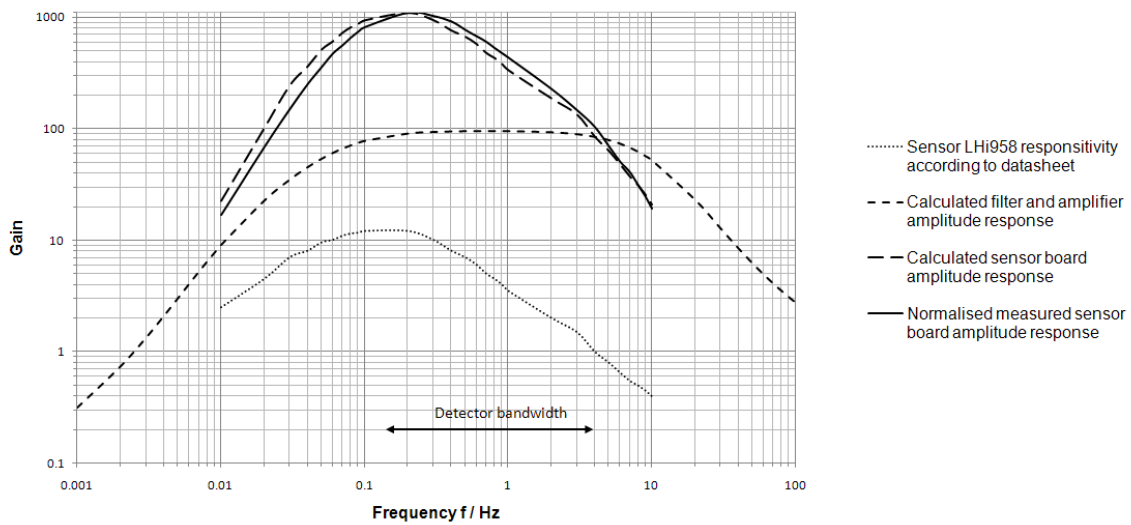


Figure 5.16: Amplitude transfer response from the v0 board

The measured amplitude response from the test assembly is also shown in Figure 5.16 and called 'normalised measured sensor board amplitude response'.

The calculated frequency range from the dual element detector LHi 958 in Equation 5.1 and Equation 5.2 on page 36 is between 143 mHz and 3.9 Hz . This frequency range is marked in Figure 5.16 as 'Detector bandwidth'. The graph for the 'normalised measured sensor board amplitude response' is normalised with a maximum value of 1088. This value is the maximum value from the graph 'calculated sensor board amplitude response'. The measured values can not be compared with the expected values without the normalization. Only a part from the emitted radiation from the infrared emitter, for example, reaches the detector on the v0 board.

The measured graph 'normalised measured sensor board amplitude response' is very similar

to the expected graph 'calculated sensor board amplitude response'. In conclusion the sensor board filter works as expected and passed the hardware test.

5.1.6 V1 sensor board layout

The layout problems from the v0 sensor board layout are fixed version v1. The space on the sensor board for the capacitors is adapted to the size of the components. The infrared sensor LHi 958 is rotated into a parallel direction to the board exterior. That means that the detecting direction is parallel to one of the sensor board sides. The size of the board is developed to put the board together with the Fresnel lens into a box with the dimensions $50\text{ mm} \cdot 45\text{ mm} \cdot 30\text{ mm}$. These boxes are available at the University. The corners of the board are cut to put the board into the box. The v1 sensor board layout is shown in Figure 5.17.

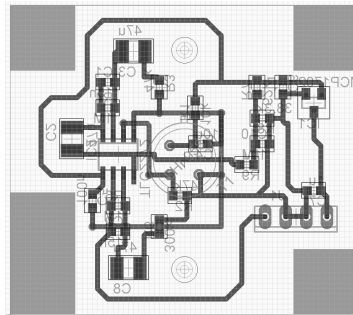


Figure 5.17: V1 sensor board layout for signal conditioning of infrared sensor LHi 958 in Eagle 5.6.0

The board was populated by hand. A photo from the top of the finished v1 sensor board is shown in Figure 5.18 and from the bottom in Figure 5.19.

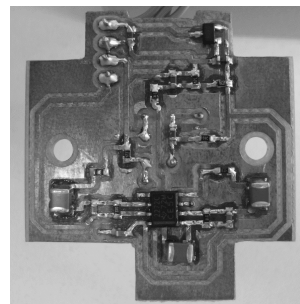
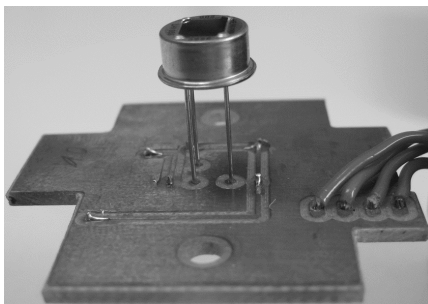


Figure 5.18: Photo from the top of the v1 sensor board
Figure 5.19: Photo from the bottom of the v1 sensor board

5.1.7 V1 sensor board hardware test

To test the v1 sensor board the same test assembly as in subsection 5.1.5 is used. The measured amplitude response of the test assembly measurement is shown in Figure 5.20 and is called 'normalised measured sensor board amplitude response'.

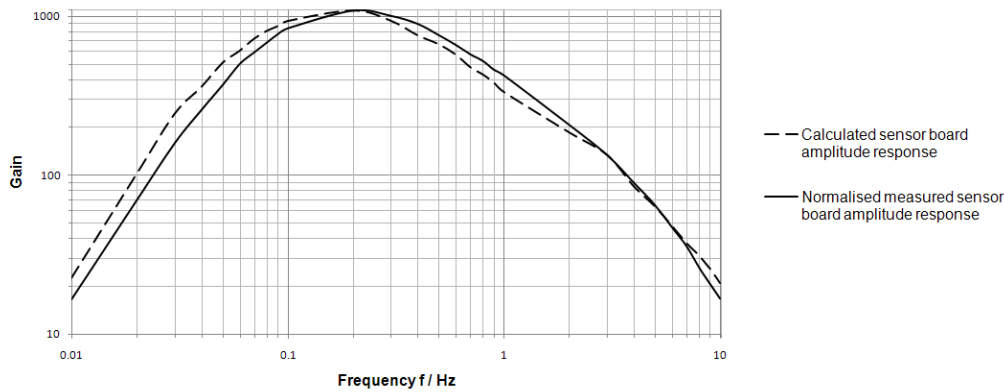


Figure 5.20: Amplitude transfer response from the v1 sensor board

The calculated amplitude response including the sensor and the electronic circuit is called 'calculated sensor board amplitude response'. The 'calculated sensor board amplitude response' is the same as in subsection 5.1.5. The graph for the 'normalised measured sensor board amplitude response' is normalised with a maximum value of 1088. This value is the maximum value from the graph 'calculated sensor board amplitude response'. The normalization makes it easier to compare the expected and the measured signals.

The 'normalised measured sensor board amplitude response' is nearly the same as the 'calculated sensor board amplitude response'. The 'measured sensor board amplitude response' is very similar to the 'measured sensor board amplitude response' from the v0 sensor board shown in Figure 5.16 on page 47. The redesign from the v0 sensor board didn't affect the functionality. The redesign solved the mechanical problems from the components, the sensor and the size of the board. In conclusion the v1 sensor board can be used as the final sensor board for the proposed sensor box.

5.1.8 Final sensor board circuit with lens in a package

To use the sensor board in an experimental environment it is necessary to put the sensor board in a box to protect it. The box protects the sensor board against radiation, mechanical stress and provides a connector to interface the box to the microcontroller. The used sensor board for this final version is the v1 sensor board.

The chosen lens in subsection 5.1.1 has to have a distance of f_b from the sensing element in the sensor. f_b is the focal length from the lens and has a value of $f_b = 4.5 \text{ mm}$. To achieve this distance a cover is used. The cover is manufactured by the technicians at Edinburgh Napier University. The lens is bonded with glue together with the cover. Figure 5.21 shows a photo from the sensor, the cover and the lens.

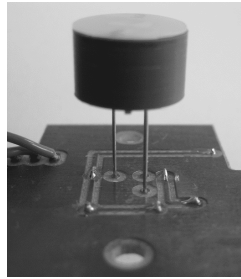


Figure 5.21: Photo from the dual element detector Lhi 958, the lens and the v1 sensor board

The box has output dimensions of $50 \text{ mm} \cdot 45 \text{ mm} \cdot 30 \text{ mm}$. On one side of the box a connector is integrated to connect the box to the microcontroller. This connector has four pins and is connected to J1, shown in Figure 5.7 on page 39, on the sensor board. The pin numbers of the connector are the same as the pin numbers of J1. The opened box with the sensor board, the lens and the connector is shown in Figure 5.22.

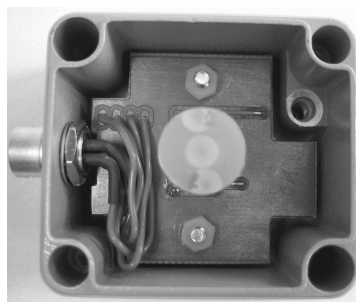


Figure 5.22: Photo from the opened sensor box

The closed box is shown in Figure 5.23.



Figure 5.23: Photo from the sensor box with connector and lens from outside

The box detects infrared radiation which is emitted by a person and transforms the signal into an analogue output signal. This output signal has a voltage range between 0 V and 2.5 V . The voltage power supply for the box should be between 4 V and 13 V according to the datasheet from the voltage regulator MCP1702T. The voltage regulator is shown in the schematic from the sensor board in Figure 5.7 on page 39. The pin configuration from the connector of the box is shown in Table 5.1.

Pin	Signal
1	positive supply voltage
2	supply ground
3	analogue ground
4	analogue signal output

Table 5.1: Pin configuration from the connector in the sensor box

5.2 Transmission of signal data

This capture describes the transmission of signal data to the computer from up to four sensor boards. The analogue output signal from one sensor box has a voltage range between 0 V to 2.5 V and a frequency range between 0 Hz and 3.9 Hz. The lower value from the frequency range is 0 Hz because the sensor board output offset voltage $V_{out\ off}$ has a frequency of 0 Hz. The higher value from the frequency range is calculated in Equation 5.2 on page 36.

This signal must be digitized to send it to the computer. To digitize a signal with a maximum frequency $f_{max} = 3.9\ Hz$ a sampling frequency $F > 7.8\ Hz$ is required, according to the Nyquist theorem.

$$F > 2 \cdot f_{max} = 2 \cdot 3.9\ Hz = 7.8\ Hz \quad (5.21)$$

The sampling rate T from the digital to analogue converter is $T < 128\ ms$.

$$T = \frac{1}{F} = \frac{1}{7.8\ Hz} = 128\ ms \quad (5.22)$$

The analogue to digital conversion can be done with a microcontroller. This microcontroller could send the digital value after the conversion to the computer. Most microcontrollers have a serial port included which sends the data to the computer. The microcontroller must be capable to send four digital values per sample rate to the computer, one digital value from each sensor box.

One value consists of four digits to represent the analogue value between 0000 mV and 2500 mV. Therefore a string of 16 *digits* per 128 ms must be send to the computer. One digit could be represented as an ASCII which consists of one byte. To send one byte via a serial port with start and stop bit 10 *symbols* are required. To transmit 16 *digits* per sample rate via the serial port 160 *symbols* per 128 ms are send. This is equivalent to a Baud Rate $B = 1.25\ kBd$

$$B = \frac{160\ symbols}{128\ ms} = 1250\ \frac{symbols}{s} = 1.25\ kBd \quad (5.23)$$

A serial connection offers much higher Baud Rates than $B = 1.25\ kBd$. In conclusion for the transmission of the signal data from the microcontroller to the computer the serial port will be fast enough to transmit all the data. Edinburgh Napier University has a microcontroller from Silicon Labs in a development kit available. In the next subsection the development kit will be analysed.

5.2.1 Microcontroller Development Kit

Edinburgh Napier University has the development kit with the type number C8051F350DK from Silicon Labs available. This development kit comes with the Silicon Labs Integrated Development Environment, an USB Debug Adapter and a Target Board. This subsection describes the parts from the development kit which are important for the application. More information about the development kit or about the microcontroller are available in the manuals [16] and [17]. The Target Board contains the microcontroller C8051F350, voltage regulators, two buttons, two LED's and the RS-232 transceiver SP3223ECY. This transceiver connects the RS232 serial port from the computer with the microcontroller on the Target Board. The Target Board is shown in Figure 5.24.

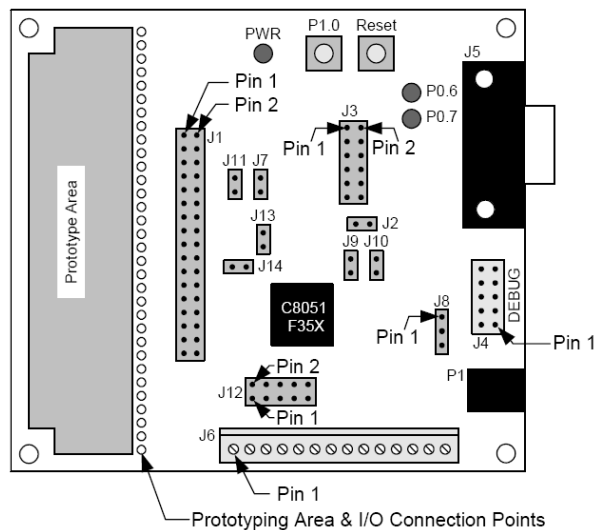


Figure 5.24: Targeted Board from the development kit C8051F350DK from Silicon Labs [16]

The relevant short cuts from the Target Board are mentioned below:

- P1 Power connector
- J1 22-pin Expansion I/O connector
- J4 DEBUG connector for Debug Adapter interface
- J5 DB-9 connector for UART0 RS232 interface
- J6 Analogue I/O terminal block

5.2.2 Microcontroller C8051F350

The microcontroller C8051F350 is from the 'Precision Mixed-Signal' family. This family offers high-precision analogue data converters with a high-throughput. The features from the microcontroller C8051F350 are described below. More information about the features is available in the microcontroller manual [17].

Features from the microcontroller C8051F350:

- One 24 bit analogue to digital converter with eight multiplexed (AMUX) analogue inputs
- Two 8 bit current mode digital to analogue converter (IDAC)
- Two voltage references, one internal 2.5 V voltage reference and one external voltage reference
- One temperature sensor
- One voltage comparator
- 12 interrupts with two priority levels
- Flash memory and external RAM
- One internal 24.5 MHz oscillator and one external oscillator drive circuit
- 17 Input and Output pins which can be organized (CROSSBAR) as analogue or digital pins
- Programmable Counter Array (PCA) which provides enhanced timer functionality
- System Management Bus (SMBus); Two-wire, bi-directional serial bus
- Universal asynchronous receiver/transmitter (UART); Asynchronous, full duplex serial port
- Serial Peripheral Interface (SPI) which provides access to a flexible, full-duplex synchronous serial bus
- Four 16 bit timers/counters
- C2 on-chip Silicon Labs 2-wire debug interface to allow Flash programming

The two most important features for this application are the 24 bit analogue to digital converter and the Universal asynchronous receiver/transmitter (UART0). The following two subsections will explain these two features more in detail.

5.2.3 24 bit analogue to digital converter

The microcontroller C8051F350 has one 24-bit analogue to digital converter (ADC0) with multiplexed analogue inputs. The ADC0 measures the voltage difference between AIN+ and AIN- as shown in Figure 5.25. The analogue inputs AIN+ and AIN- can be multiplexed to the analogue input pins (AIN0.x), to analogue ground (AGND) or to the internal temperature sensor.

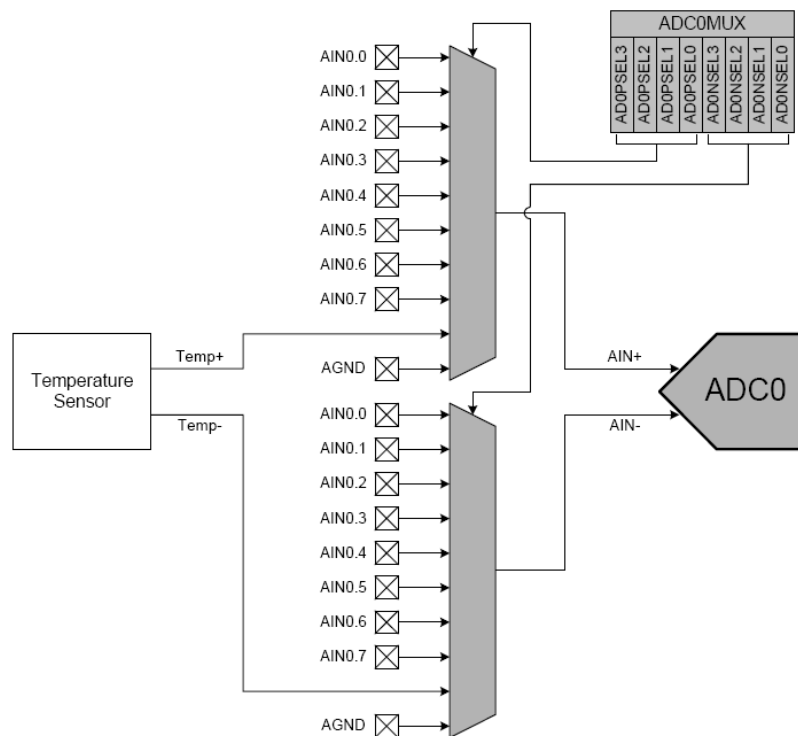


Figure 5.25: Connections for the multiplexer from the analogue to digital converter [17]

To configure the multiplexer the register ADC0MUX is used which is an eight bit register. The first four bits are to configure AIN- and the last four bits to configure AIN+. For example to connect AIN- with AGND and AIN+ with AIN0.0 the register ADC0MUX must be load with 0x08. 8 mean that AGND is connected to AIN- and 0 means that AIN0.0 is connected to AIN+. For the application it is necessary to measure the analogue voltage from four inputs. Each of the four inputs is connected to one sensor board. AIN- is connected to AGND and AIN+ changes between AIN0.0, AIN0.1, AIN0.2 and AIN0.3 to multiplex the signal for the ADC0. To measure the analogue signal from these four inputs the ADC0MUX configuration in Table 5.2 is necessary.

AIN+	AIN-	ADC0MUX
AIN0.0	AGND	0x08
AIN0.1	AGND	0x18
AIN0.2	AGND	0x28
AIN0.3	AGND	0x38

Table 5.2: ADC0MUX register values from the microcontroller to configure the multiplexer

Program code in C to switch between the four analogue inputs is given in the function `switchToNextInput()`. The input after AIN0.3 is AIN0.0.

```
void switchToNextInput (void)
{
    // get actual analogue input
    int actual_analogue_input = (ADC0MUX & 0xF0) » 4;
    // switch to the next analogue input
    if (3 > actual_analogue_input)
        ADC0MUX = ((actual_analogue_input + 1) « 4) | 0x08;
    else ADC0MUX = 0x08;
}
```

The time to switch between the analogue inputs must be longer than the time constant to reload the input capacities.

The output AIN+ and AIN- from the multiplexer is connected to the input of the ADC0. The analogue to digital converter has burnout current sources, input buffers, an offset digital analogue converter, a programmable gain amplifier (PGA), a modulator to digitize one sample and filters. The block diagram from the ADC0 is shown in Figure 5.26.

The analogue input voltage range between AIN+ and AIN- is between 0 V and +VREF. +VREF is the voltage reference for the modulator. The microcontroller has an internal 2.5 V VREF source. As the sensor box has an output voltage range between 0 V and 2.5 V the internal 2.5 V VREF source can be used as reference. Moreover the target board has one 2.5 V voltage regulator included to set this voltage as an external reference. In conclusion the input voltage range between AIN+ and AIN- is between 0 V and 2.5 V.

The burnout current sources can be enabled with the ADC0BCE bit. If enabled the positive channel source sources 2 μA on AIN+ and the negative channel source sources $-2 \mu A$ on AIN-.

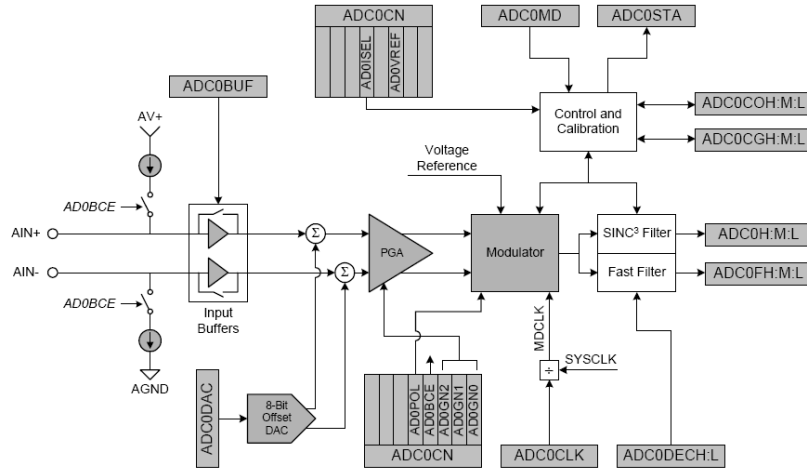


Figure 5.26: Analogue to digital converter ADC0 block diagram [17]

The burnout current sources can be used to detect an open or short circuit connected to AIN+ and AIN-. While an analogue to digital conversion the burnout current sources should be disabled.

After the burnout current sources the signals can be buffered with input buffers to minimize the input current for sensitive measurements. Without the input buffers the input impedance between AIN+ and AIN- is $R = 7 \text{ M}\Omega$. This is equivalent to a maximum input current from $I_{max} = 358 \text{ nA}$.

$$I_{max} = \frac{U_{max}}{R} = \frac{2.5 \text{ V}}{7 \text{ M}\Omega} = 358 \text{ nA} \quad (5.24)$$

The maximum input current I_{max} with enabled input buffers is $I_{max} = 30 \text{ nA}$. The output from the sensor box can supply the analogue to digital converter with more than $I = 358 \text{ nA}$. In conclusion the input buffers are not necessary for this application.

After the input buffers a voltage offset can be added to the signal. An 8 bit digital to analogue converter (DAC) is included to add ± 0.5 of the ADC's voltage input range to the signal. The ADC0DAC register controls the offset voltage. The output voltage signal from the sensor board is between 0 V and 2.5 V . This is the same range as the ADC can digitise and therefore it is not necessary to add a voltage offset.

After the 8 bit offset DAC the signal can be amplified with a programmable gain amplifier (PGA). The PGA can be controlled with the three AD0GN0/1/2 bits. The amplifier provides amplifications of 1,2,4,8,16,32,64 and 128. As the output signal from the sensor box is between 0 V and 2.5 V it is not necessary to amplify the signal.

The next step for the signal is the delta sigma modulator to digitise the analogue input signal.

5 Proposed design

As mentioned above the voltage reference for the modulator is $2.5 V$. The modulator clock ($MDCLK$) determines the switching frequency for the sampling capacitors. The $ADC0CLK$ register divides the system clock $SYSCLK$ to get the modulator clock. The optimal value for the modulator clock is $MDCLK = 2.4576 MHz$ [17]. The modulator samples the input signal at a sample rate of $\frac{MDCLK}{128}$. Therefore the sample rate is $\frac{2.4576 MHz}{128} = 19.2 kHz$. The delta sigma modulator is controlled by control and calibration registers.

After digitizing the signal with the modulator there are two different filters to filter the signal. The output word from the filters is stored in the 24 bit register $ADC0H:M:L$ or $ADC0FH:M:L$ depending on the selected filter. The decimation ratio in register $ADC0DECH:L$ determines how many modulator samples are used to generate a single output word. The minimum amount of modulator samples are 20 for both filters. The two filters Fast Filter and SINC3 Filter are available. The Fast Filter produces after the decimation ratio defined samples one output word. The SINC3 Filter needs three times longer to determine one output word with the same decimation ratio. The output noise from the Fast Filter is much higher than the output noise from the SINC3 Filter. For example for a decimation ratio of 192 and a PGA gain setting from 1 the Fast Filter has a typical RMS Noise of $550.29 \mu V$ and the SINC3 Filter of $13.1 \mu V$. For a decimation ratio from 20 the SINC3 Filter produces a typical RMS Noise of $2974 \mu V$. For more details see the user's manual [17]. If possible it is better to use the SINC3 Filter to get lower noise output words.

The highest throughput $f_{tp_{max}}$ of the analogue to digital converter is therefore the sample rate divided by the minimum decimation ratio.

$$f_{tp_{max}} = \frac{f_{sample}}{dec_{ratio_{min}}} = \frac{19.2 kHz}{20} \approx 1 kHz \quad (5.25)$$

The $ADC0$ offers single conversion's and continuous conversion's. Single conversion means that the conversion is initiated after writing the ADC system mode bits ($AD0SM$) to single conversion. At the end of the conversion the ADC system mode becomes idle. Now the conversion can start again by setting the $AD0SM$ bits to single conversion.

Continuous conversion means that the conversion is initiated after writing the ADC system mode bits to continuous conversion. From now the $ADC0$ produces output words. After each conversion the output registers are updated and the $AD0INT$ interrupt bit is set to 1. To stop the continuous conversion mode the system mode bits have to be written to idle mode.

To read after each conversion from another input it is necessary to change the $ADC0MUX$ register from the multiplexer. This register should only be modified when the system is in idle mode. As the continuous conversion doesn't return after a conversion to idle mode it is convenient to use the single conversion for multiple input signals. The single conversion returns

after each conversion to the idle mode.

To read the four analogue input signals it is necessary to set the multiplexer settings in idle mode before each single conversion. Figure 5.27 shows the operating states for single conversion from various analogue input signals. After setting the analogue input in the ADC0MUX register the single conversion starts. When the conversion finishes the AD0INT interrupt occurs and the output word is send to the PC. Now the next analogue input is set and the same starts again.

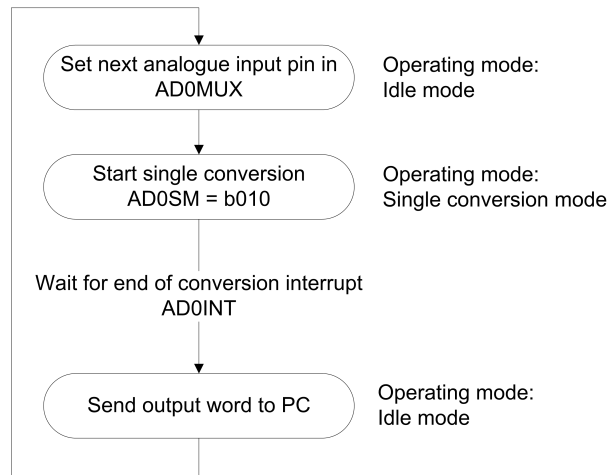


Figure 5.27: Operating states for single conversion mode with various analogue input signals

The digitized output signal from the microcontroller is displayed on the computer as a graph with up to four series. The microcontroller should always work with the same output word rate uninfluenced by the number of captured input signals. Therefore it is not necessary to determine the time on the computer between two output words. The output word rate must be higher than $f_{tp_{min}} = 7.8 \text{ Hz}$ for each channel to digitize the analogue signals like calculated in Equation 5.21 on page 52. The output word rate f_{tp} for the SINC3 filter is determined by the decimation ratio ADC0DEC, the modulator sample rate f_{sample} and the number of captured analogue inputs inp .

$$f_{tp} = \frac{f_{sample}}{ADC0DEC} \cdot \frac{1}{3} \cdot \frac{1}{inp} \quad (5.26)$$

The highest output word rate $f_{tp_{max}}$ for four inputs and the SINC3 filter is $f_{tp_{max}} = 80 \text{ Hz}$.

$$f_{tp_{max}} = \frac{f_{sample}}{ADC0DEC_{min}} \cdot \frac{1}{3} \cdot \frac{1}{inp} = \frac{19.2 \text{ kHz}}{20} \cdot \frac{1}{3} \cdot \frac{1}{4} = 80 \text{ Hz} \quad (5.27)$$

The microcontroller has an internal value for the output word rate OWR , which is not the

external output word rate f_{tp} .

$$OWR = \frac{f_{sample}}{ADC0DEC} \quad (5.28)$$

The OWR doesn't depend on the used filter or the number of analogue inputs. For $OWR = 800 \text{ Hz}$ the decimation ratio is $ADC0DEC = 24$. Therefore $f_{tp} = 66.6 \text{ Hz}$ for four inputs which are filtered with the SINC3 filter. The value for the output word rate $f_{tp} = 66.6 \text{ Hz}$ is between $f_{tp_{min}} = 7.8 \text{ Hz}$ and $f_{tp_{max}} = 80 \text{ Hz}$. The ADC will work with the output word rate

$$f_{tp} = 66.6 \text{ Hz} \quad (5.29)$$

to digitize the four analogue input signals.

To have always the same output word rate f_{tp} , the decimation ratio $ADC0DEC$ must be changed depending on the number of analogue inputs.

$$ADC0DEC = \frac{f_{sample}}{f_{tp}} \cdot \frac{1}{3} \cdot \frac{1}{inp} \quad (5.30)$$

This is equal to a change of the output word rate OWR .

$$OWR = f_{tp} \cdot 3 \cdot inp \quad (5.31)$$

$$OWR_{(inp=1)} = 66.6 \text{ Hz} \cdot 3 \cdot 1 = 200 \text{ Hz} \quad (5.32)$$

$$OWR_{(inp=2)} = 66.6 \text{ Hz} \cdot 3 \cdot 2 = 400 \text{ Hz} \quad (5.33)$$

$$OWR_{(inp=3)} = 66.6 \text{ Hz} \cdot 3 \cdot 3 = 600 \text{ Hz} \quad (5.34)$$

$$OWR_{(inp=4)} = 66.6 \text{ Hz} \cdot 3 \cdot 4 = 800 \text{ Hz} \quad (5.35)$$

This means the output signal noise is higher for four inputs than for one input because the decimation ratio is lower. For $OWR = 960 \text{ Hz}$ the typical RMS noise is $2974 \mu V$ and for $OWR = 240 \text{ Hz}$ the typical RMS noise is $93.2 \mu V$. For more values of the typical RMS noise see the microcontroller manual [17]. According to the mentioned RMS noise a digital value resolution of 1 mV is sufficient. After the conversion the digital value is represented with four digits between 0000 mV and 2500 mV .

5.2.4 Universal asynchronous receiver/transmitter

The microcontroller has one universal asynchronous receiver/transmitter (UART0). This UART0 on the target board is connected to the RS-232 transceiver SP3223ECY. The transceiver changes the voltage level of the serial UART0 signal to an RS-232 voltage level. Figure 5.28 shows the

connection between PC and microcontroller.

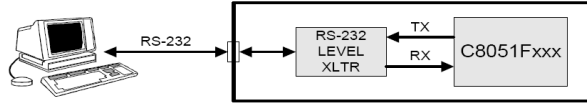


Figure 5.28: RS-232 connection between the PC and the microcontroller [17]

The UART0 has two operational modes, 8-Bit UART and 9-Bit UART. The 8-Bit UART mode sends one start bit, eight data bits and one stop bit. The 9-Bit UART mode sends one start bit, nine data bits and one stop bit. In this case the 8-Bit UART mode is convenient because one byte consists of 8 bit and the program will be based on bytes. The 8-Bit UART mode bit sampling is shown in Figure 5.29.

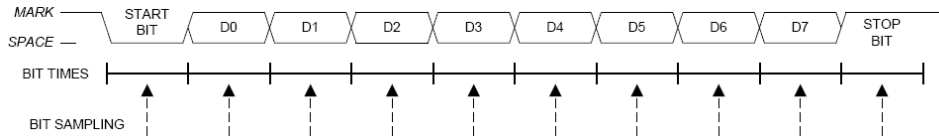


Figure 5.29: 8-Bit UART mode bit sampling [17]

To send the value 2123 via RS232 to the computer four bytes are required if each digit is represented as an ASCII. One ASCII is represented with 8 bits. Therefore to send this four digits with start and stop bit included the UART0 has to send $4 \cdot 10 \text{ symbols} = 40 \text{ symbols}$.

The UART0 offers different Baud Rates which are generated by Timer 1 in 8-bit auto-reload mode. The minimum Baud Rate B_{min} is calculated in Equation 5.23 on page 52 as $B_{min} = 1.25 \text{ kBd}$. For the application a Baud Rate $B = 115.2 \text{ kBd}$ is used. This Baud rate was chosen because it is capable to send all the data in a shorter time to the computer. A lower Baud Rate would be enough for this application.

The time to send one symbol t_{sym} is the reciprocal value from the Baud Rate. The symbol time t_{sym} for a Baud Rate $B = 115.2 \text{ kBd}$ is $t_{sym} = 8.68 \mu s$.

$$t_{sym} = \frac{1}{B} = \frac{1}{115.2 \text{ kBd}} = 8.68 \mu s \quad (5.36)$$

Silicon Laboratories offers in their IDE the functions `printf(...)` and `getkey()`. `Printf()` sends data to the RS-232 serial port. `Getkey()` waits to receive one byte from the RS-232 serial port. Both functions do all the UART0 interrupt handling and data buffering.

To send the digitized values to the computer start and stop tags are required to inform the software about the first and the last value from a conversion cycle. The start tag is a 'B' and

the stop tag an 'E'. The microcontroller sends the start tag before the first digitized value and the stop tag after the last digitized value. To send digital input information from the microcontroller to the PC the D-byte is reserved which is send after the start tag. The data which is send to the computer, including start and stop tag, is called frame. Figure 5.30 shows the frame for one digitized value and Figure 5.31 for four digitized values.

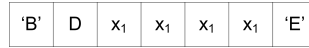


Figure 5.30: RS-232 frame for one digitized value

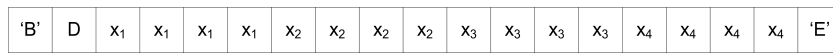


Figure 5.31: RS-232 frame for four digitized values

The first and the last byte are start and stop tag. The D-byte contains information about the digital input state from some digital inputs. The x-bytes are the digitized analogue input values. To send the frame in Figure 5.31 with a Baud Rate $B = 115.2 \text{ kBd}$ it takes $t_{send} = 1.65 \text{ ms}$.

$$t_{send} = t_{sym} \cdot symbols = t_{sym} \cdot 19 \text{ byte} = t_{sym} \cdot 190 = 8.68 \mu s \cdot 190 = 1.65 \text{ ms} \quad (5.37)$$

The output word rate from the ADC0 is $f_{tp} = 66.6 \text{ Hz}$, see Equation 5.29 on page 60. This means that the microcontroller prepares each $t_{tp} = 15 \text{ ms}$ one frame. The time to send the frame to the computer t_{send} must be equal or less than the conversion time t_{tp} . To send one frame with information about all four analogue inputs a sending time from $t_{send} = 1.65 \text{ ms}$ is required. This is less than the conversion time $t_{tp} = 15 \text{ ms}$.

5.2.5 Implemented Firmware on the microcontroller

The microcontroller is connected between the sensor boxes and the computer. It digitizes the sensor box output signals and sends them via the serial port to the computer.

The firmware is capable to convert up to four analogue inputs with the output word rate $f_{tp} = 66.6 \text{ Hz}$. Depending on the number of used analogue inputs the signal noise after the conversion changes. Lower analogue inputs means less output noise. The microcontroller sends the state from digital inputs P1.0 and P0.0 with the D-byte (see Figure 5.30) to the computer. P1.0 is connected to button S2 and P0.0 to digital infrared motion sensor AMN11112. This sensor is a passive infrared detector with a digital output signal. The D-byte is displayed in ASCII code and the possible values are shown in Table 5.3.

P1.0	P0.0	D-byte
OFF	OFF	0
OFF	ON	1
ON	OFF	2
ON	ON	3

Table 5.3: D-byte values including the state of digital inputs P1.0 and P0.0

To reset the microcontroller the external reset button can be pressed or the SWRSF bit must be set to one. The SWRSF is the software reset force bit in register RSTSRC. After a reset of the microcontroller the firmware starts to initialize the system clock, then the input and output ports and then the UART0. Now the controller waits to receive one byte from the computer via UART0. This byte informs the microcontroller about the amount of analogue inputs or forces it to make another reset. Table 5.4 shows the accepted byte values.

Received byte	Interpretation
0x30	Reset microcontroller
0x31	Read one analogue input (A0.0)
0x32	Read two analogue inputs (A0.0,A0.1)
0x33	Read three analogue inputs (A0.0,A0.1,A0.2)
0x34	Read four analogue inputs (A0.0,A0.1,A0.2, A0.3)

Table 5.4: After a microcontroller reset the microcontroller waits for a byte on the UART0 serial port to set the number of analogue inputs. This table contains the accepted values for this byte.

The function `getkey()` waits for one byte in the UART0 input buffer and gives this byte as return value to the application. The code cut-out of this part is shown followed.

```
switch (getkey ()) {
    case 0x30: // reset microcontroller
        RSTSRC |= 0x10; // Reset System
        break;
    case 0x31: // read 1 analogue input
        amount_of_analogue_inputs = 1;
        OWR = 200;
```

```

    break;
    ...
}

```

If the microcontroller receives a valid byte the analogue to digital converter ADC0 initialises. Now the firmware sends each 15ms one output frame via UART0 to the computer. This frame is send with the printf() function. The firmware uses the SINC3 filter in single conversion mode.

It is possible to reset the microcontroller via software or to toggle the digital output P0.6. P0.6 is connected to LED D2 on the Target board. Both can be achieved via UART0. The accepted byte values from the microcontroller are shown in Table 5.5.

Received byte	Interpretation
0x30	Reset microcontroller
0x39	Toggle digital output P0.6

Table 5.5: While the microcontroller sends frames to the computer the microcontroller can be reset or the digital output P0.6 can be toggled. The accepted byte values on UART0 are shown in this table

The digital output P0.6 can be toggled while the microcontroller digitises the analogue inputs.

5.3 Graphical display in a Windows environment

The software on the computer displays up to four digitized analogue signals at the same time like an oscilloscope. The software receives the data via the serial RS-232 port. The data format is explained in the section before. The program runs on a Windows environment with Windows XP as the operating system. This is the most common operating system and installed on a huge amount of computers.

Edinburgh Napier University has Visual Studio 2008 installed. This software has an IDE with source code editor, compiler and debugger. Furthermore Visual Studio 2008 has a toolbox with amongst others forms, buttons, timers and serial port code blocks. It provides the programming languages Visual Basic, C# and C++. The source code for the application is written in C++. C++ is a common object orientated language to implement software.

The Microsoft Developer Network [18] provides the .Net Framework which can be installed on a Microsoft Windows operating system. The .Net Framework offers a huge amount of coded solutions. Most of the used classes in this project are from the .Net Framework.

5.3.1 Connection to serial port

To include a serial port the class `System::IO::Ports::SerialPort` is used. This class represents the serial port and provides methods to send and read data. The following example shows how to use this class.

```
// Create a SerialPort for COM1 with 8 data bits and a Baud Rate of B=115.2 kBd
System::IO::Ports::SerialPort com_port;
com_port = gnew System::IO::Ports::SerialPort();
com_port->BaudRate = 115200;
com_port->DataBits = 8;
com_port->PortName = "COM1";
// Connect to COM1
this->com_port->Open();
// Read from COM1
String read_from_comport;
read_from_comport = this->com_port->ReadExisting();
```

The microcontroller sends each 15 *ms* a frame to the computer which must be read continuously.

The self implemented class `Comfrei` offers the methods `void open(int comport)`, `void close(void)`, `System::String^ getframe(void)` and `void sendframe(System::String^ string)`. With `open('1')` the software connects to the serial port COM1 and with the call of the method `close()` the serial

port closes. The method `getframe()` has as return value a string which consists of one frame without start and stop tag. This method should be called minimum each 15 *ms* to clear the input buffer. With the method `sendframe('0')` the computer sends a string to the microcontroller. In this case ASCII '0' is equally to 0x30 and resets the microcontroller. See Table 5.4 on page 63 and Table 5.5 on page 64 for more details.

After the start of the program there are two buttons available. One button is to change the COM Port and the button Start is to connect the software with the serial COM Port. With a click on button Stop the application stops and disconnects the serial port.

5.3.2 Microsoft chart controls

To plot the received data in a chart on the computer Microsoft provides its customers additional packages to download. One of these packages is the Microsoft Chart Controls for Microsoft .NET Framework 3.5. This package is capable to plot a chart. To use the package the .NET Framework 3.5 SP1 must be installed and to include it into Visual Studio the package Microsoft Chart Controls Add-on for Microsoft Visual Studio 2008 is required. All these packages are available on the Microsoft Download Center [19].

The software uses the class `System::Windows::Forms::DataVisualization::Charting::Chart` from Microsoft Chart Controls to visualises data in a graph. This documentation doesn't explain how to use this class. Additional information are available on the Microsoft Developer Network [18]. The self written class `Chartfrei` offers methods to plot the graph and uses the class `System::Windows::Forms::DataVisualization::Charting::Chart`.

The method `void add_values_to_series(int analogue_value_AIN[], int average_value, int amount_of_series)` adds new values to the graph. This method adds data points on the right side of the chart and deletes data points on the left side if the chart is full. The variable `amount_of_series` tells the chart how many series must be displayed and according to this information the content of the array `analogue_value_AIN[]` and the variable `average_value` is plotted.

5.3.3 Software functionality

After the connection to the serial port the software reads each 15 *ms* one frame from the serial port. Afterwards the frame interpretation starts. The status from the digital inputs P0.0 and P1.0 are displayed in the main window as a radio button and the received digitized analogue values are added to the graph. For the first analogue value the software calculates the average value and plots it too. The software offers buttons to toggle the LED D2 from the microcontroller and to change the amount of captured analogue inputs on the microcontroller.

The software can be configured for digital or analogue motion detection. If motion is detected the software plots 'motion detected'. The digital motion detection bases on the information from the digital input P0.0. This input is connected to a digital motion sensor as explained in subsection 5.2.5. The analogue motion detection bases on the digitized signal from the infrared board connected to A0.0. For this input the software calculates the average value which should be around $1.25V$ as calculated in Equation 5.3 on page 37. This is the offset voltage from the sensor board. If the difference between the average value and A0.0 is higher than the threshold motion is detected.

The software has a direction detection implemented. The direction detection can detect if a person moves from the right side to the left side or from the left side to the right side. This feature works only for the analogue input A0.0. How the analogue output signal looks like is explained in Subsection 5.1.2 on page 35. Figure 5.32 shows the signal from analogue input A0.0 and the average value from A0.0 while a person moves from the right to the left. The self implemented class `Direction_detection` is used to detect the moving direction of a person. The detected direction is displayed in the main window as an arrow. The method `int add(int value)` is called after each received frame to add an analogue value to the class `Direction_detection`. The return value of this method gives information about the direction. The class `Direction_detection` integrates about the area A1, than A2 and then A3 like shown in Figure 5.32. If A1 is negative and A2 positive a movement from the right side to the left side is detected. If A1 is positive and A2 is negative a movement from the left side to the right side is detected. If there are more movements the software cannot handle this. More movements are detected if after the area A3 the signal produces an area A4. After successful direction detection the software is ready to detect a new direction. While the software detects a direction the text 'Processing' instead of an arrow is displayed.

The software has a configuration menu. In this menu it is possible to switch the plot on or off, to turn the average calculation on or off, to set the movement detection to digital or analogue, to switch the direction detection on or off, to switch an information label on or off. The information label plots same internal variables like the values from the detected areas A0 to A4, the amount of analogue inputs, a counter value for the detected directions and the amount of values in the queue for the average calculation. The value for the queue is reset if the maximum queue size is reached.

In further studies this software could be modified to add more functionality. Like for example the direction detection based on all four analogue input signals.

5 Proposed design

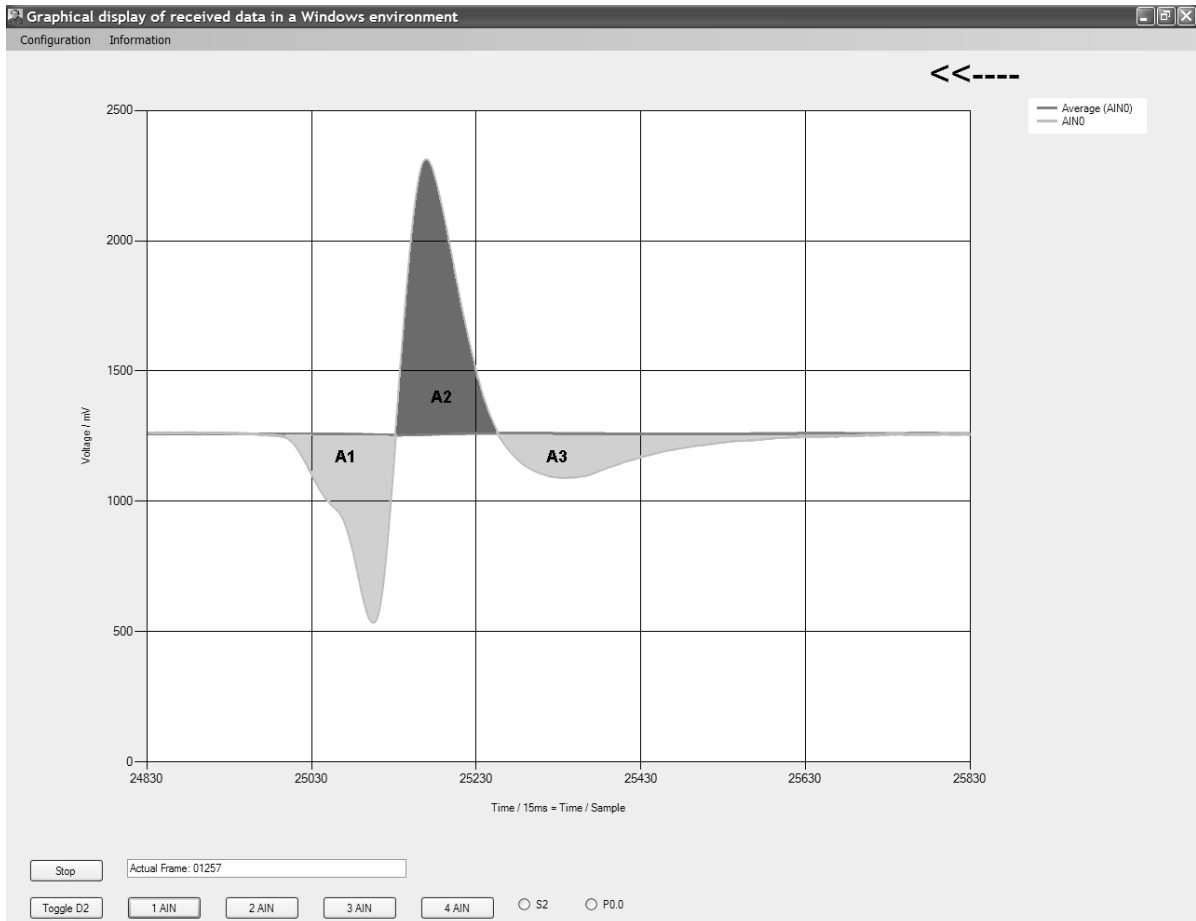


Figure 5.32: Signal from a person moving from the right to the left side. The areas A1, A2 and A3 are the detected areas. The software integrates about the detected areas.

6 Sample applications

The main application for the developed experimental kit is to analyse the sensor box output signals to combine them with algorithms. These algorithms could for example record movement profiles from a person. The implementation of these algorithms could be done in further investigations and is out of the scope of this thesis.

This chapter describes the output signal on the personal computer software while one person walks in the monitored area. For the first sample application there is only one sensor box in use and for the second sample application there are four sensor boxes in use.

The sensor boxes are connected to the microcontroller and the microcontroller to the personal computer like shown in Figure 5.1 on page 33.

6.1 Output signal of one sensor box

The sensor is installed on the ceiling of the room in a height of 2.70 m . The moving person has a height of 1.80 m . Therefore the working distance L between the person and the sensor box is $L = 2.70\text{ m} - 1.80\text{ m} = 90\text{ cm}$. Three experiments with different walking speeds v_b had been made. To measure the walking speed v_b of the person a stopwatch is used.

Figure 6.1 shows the output signal from a person with a walking speed $v_b = 1.2\frac{\text{m}}{\text{s}}$, Figure 6.2 shows the output signal from a person with a walking speed $v_b = 1.8\frac{\text{m}}{\text{s}}$ and Figure 6.3 shows the output signal from a person with a walking speed $v_b = 2.1\frac{\text{m}}{\text{s}}$. In the Figures 6.1 and 6.3 the person walks in the same direction. In Figure 6.2 the person walks in the opposite way.

The main differences between the three signals are the signal duration, signal form and amplitude. A higher walking speed means a shorter signal duration. This is because the residence time in the detection area of the sensor is shorter if the person walks faster.

The signal form depends on the moving direction of the person. The output signal has its first extreme value in the positive or negative depending on the walking direction. The difference is shown in Figure 6.2 compared with Figure 6.3. The walking direction is oppositely in these both signals.

The amplitude of the signal is also related to the walking speed v_b of the person. The Equation 3.4 on page 26 relates the sensor box output frequency f_{sens} with the walking speed

6 Sample applications

v_b of the person. The focal length is $f_b = 4.5 \text{ mm}$, the working distance between the person and the sensor box is $L = 0.9 \text{ m}$ and the size of the sensing element is $s = 1 \text{ mm}$. The sensor box output frequency for the three walking speeds is calculated in the following three equations.

$$f_{sens(v_b=1.2 \frac{m}{s})} = \frac{v_b \cdot f_b}{2\pi \cdot s \cdot L} = \frac{1.2 \frac{m}{s} \cdot 4.5 \text{ mm}}{2\pi \cdot 1 \text{ mm} \cdot 0.9 \text{ m}} = 0.95 \text{ Hz} \quad (6.1)$$

$$f_{sens(v_b=1.8 \frac{m}{s})} = \frac{1.8 \frac{m}{s} \cdot 4.5 \text{ mm}}{2\pi \cdot 1 \text{ mm} \cdot 0.9 \text{ m}} = 1.43 \text{ Hz} \quad (6.2)$$

$$f_{sens(v_b=2.1 \frac{m}{s})} = \frac{2.1 \frac{m}{s} \cdot 4.5 \text{ mm}}{2\pi \cdot 1 \text{ mm} \cdot 0.9 \text{ m}} = 1.67 \text{ Hz} \quad (6.3)$$

According to the 'calculated sensor board amplitude response' in Figure 5.16 on page 47 the gain of the signal at different frequencies varies. The following gain values $|\underline{v}|$ at the frequencies $f_{sens} = 0.95 \text{ Hz}$, $f_{sens} = 1.43 \text{ Hz}$ and $f_{sens} = 1.67 \text{ Hz}$ are read off values from Figure 5.16.

$$|\underline{v}|_{(f_{sens}=0.95 \text{ Hz})} = |\underline{v}|_{(v_b=1.2 \frac{m}{s})} = 346 \quad (6.4)$$

$$|\underline{v}|_{(f_{sens}=1.43 \text{ Hz})} = |\underline{v}|_{(v_b=1.8 \frac{m}{s})} = 263 \quad (6.5)$$

$$|\underline{v}|_{(f_{sens}=1.67 \text{ Hz})} = |\underline{v}|_{(v_b=2.1 \frac{m}{s})} = 227 \quad (6.6)$$

The peak to peak voltage value from the signal in Figure 6.3 is $V_{peak \text{ to peak}(v_b=2.1 \frac{m}{s})} \approx 0.5 \text{ V}$. With this value as basic value the other signal peak to peak values from Figure 6.2 and Figure 6.1 can be calculated.

$$V_{peak \text{ to peak}(v_b=2.1 \frac{m}{s})} = 0.5 \text{ V} \quad (6.7)$$

$$V_{peak \text{ to peak}(v_b=1.8 \frac{m}{s})} = \frac{V_{peak \text{ to peak}(v_b=2.1 \frac{m}{s})} \cdot |\underline{v}|_{(v_b=1.8 \frac{m}{s})}}{|\underline{v}|_{(v_b=2.1 \frac{m}{s})}} = \frac{0.5 \text{ V} \cdot 263}{227} = 0.58 \text{ V} \quad (6.8)$$

$$V_{peak \text{ to peak}(v_b=1.2 \frac{m}{s})} = \frac{V_{peak \text{ to peak}(v_b=2.1 \frac{m}{s})} \cdot |\underline{v}|_{(v_b=1.2 \frac{m}{s})}}{|\underline{v}|_{(v_b=2.1 \frac{m}{s})}} = \frac{0.5 \text{ V} \cdot 346}{227} = 0.76 \text{ V} \quad (6.9)$$

The calculated values for $V_{peak \text{ to peak}(v_b=1.8 \frac{m}{s})}$ and $V_{peak \text{ to peak}(v_b=1.2 \frac{m}{s})}$ are equal to the read off values in Figure 6.2 and Figure 6.1. In conclusion the peak to peak value from the sensor box output depends on the walking speed of the person and can be calculated with the used equations.

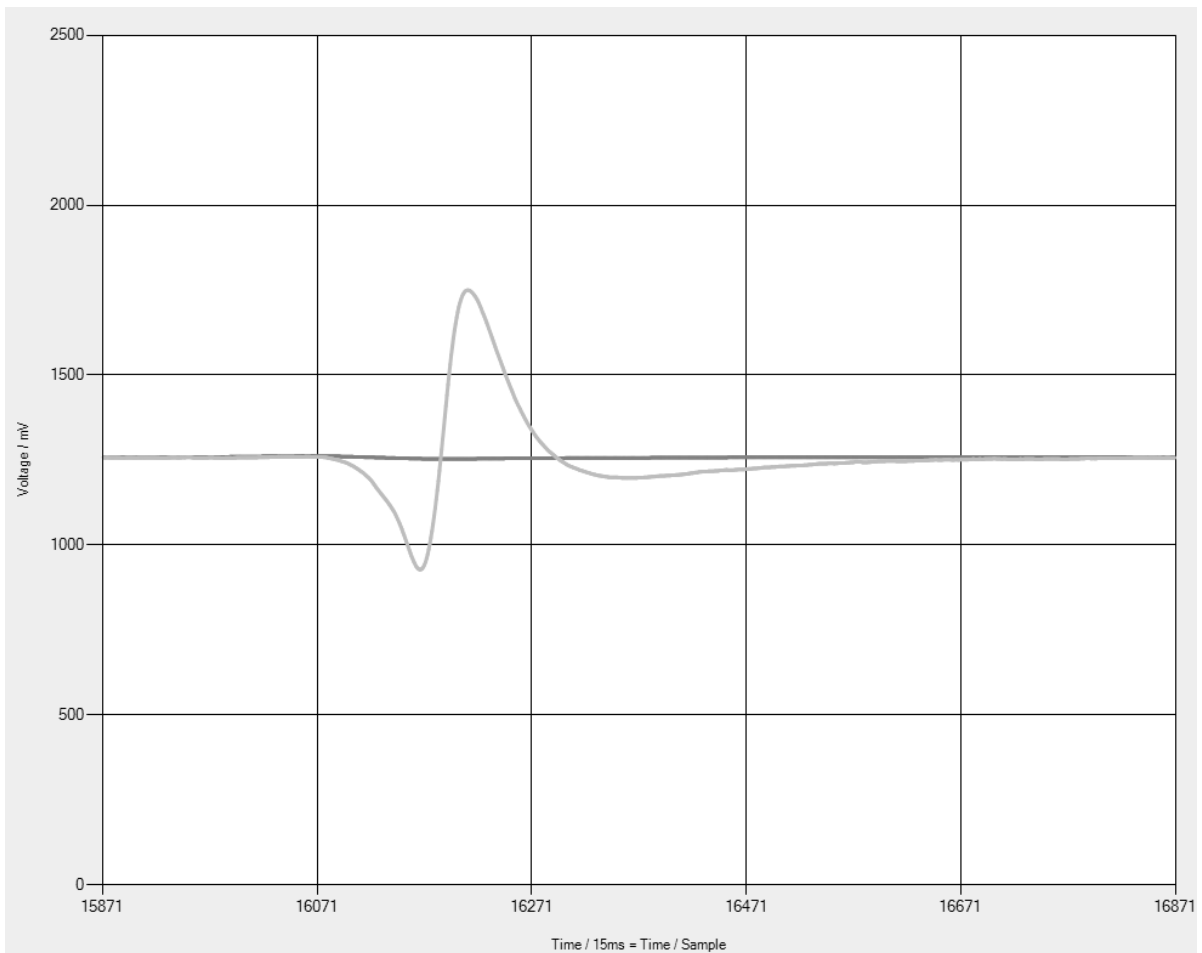


Figure 6.1: Signal from a person moving down the sensor box with a walking speed $v_b = 1.2 \frac{m}{s}$. The working distance between the person and the sensing box is $L = 90 \text{ cm}$. The graph shows *voltage / mV* versus *time / 15 ms*.

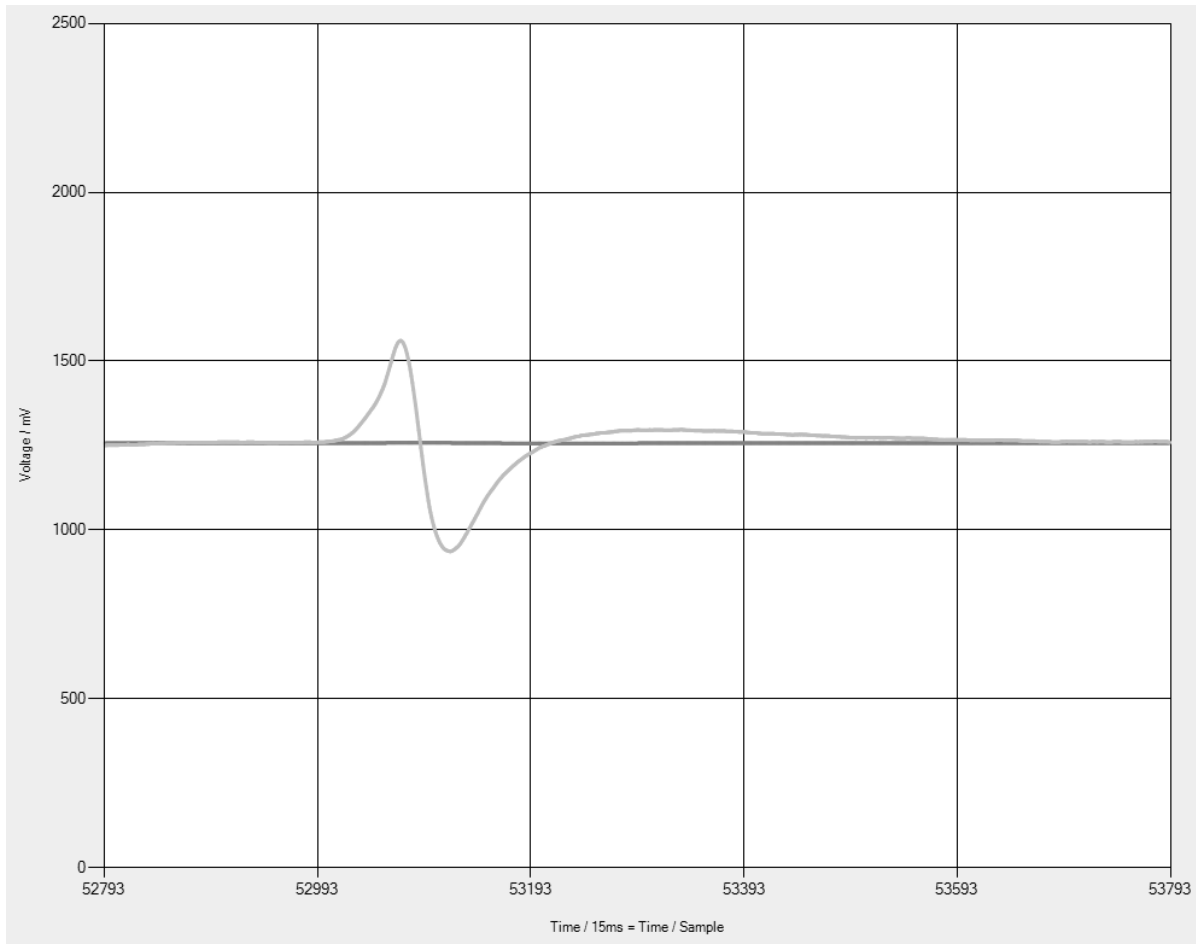


Figure 6.2: Signal from a person moving down the sensor box with a walking speed $v_b = 1.8 \frac{m}{s}$. The working distance between the person and the sensing box is $L = 90 \text{ cm}$. The graph shows *voltage / mV* versus *time / 15 ms*.

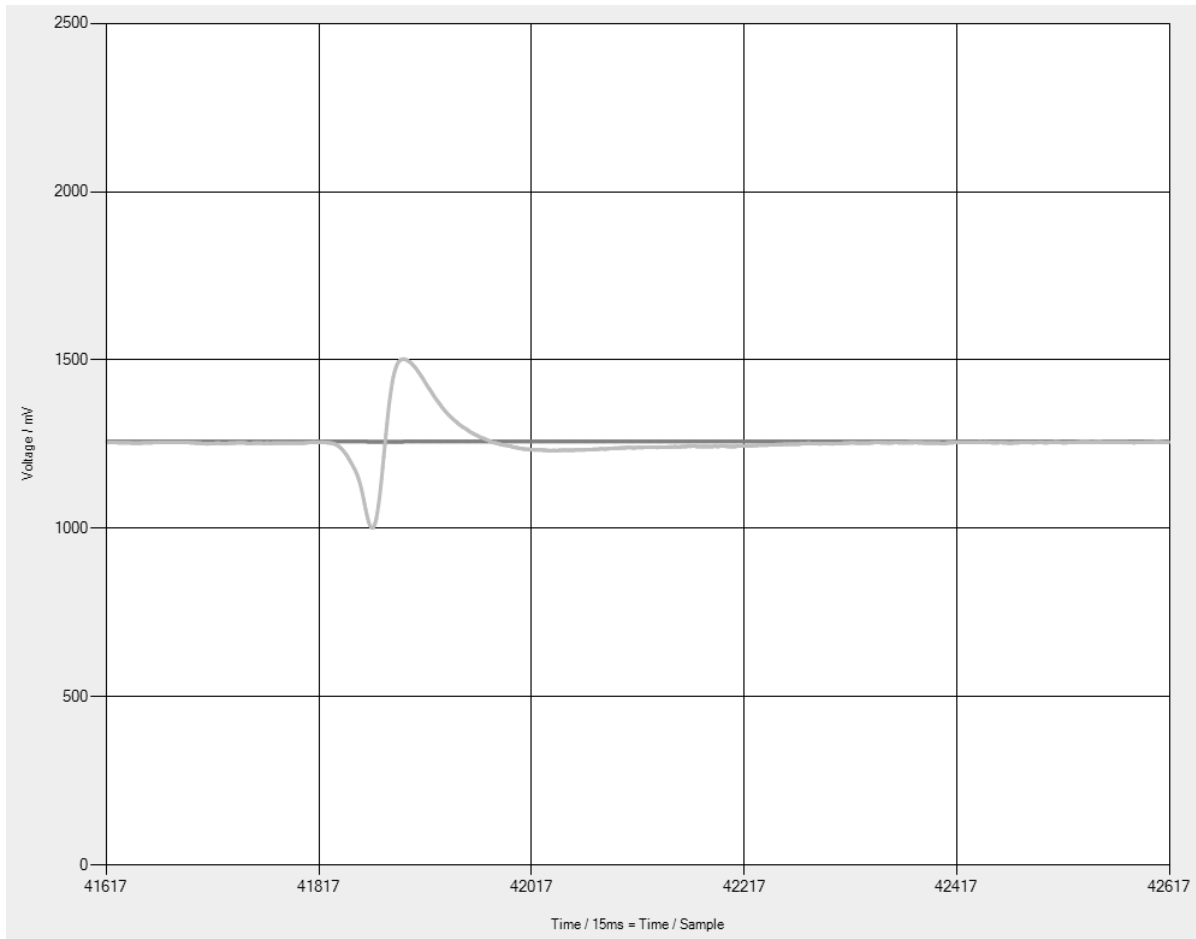


Figure 6.3: Signal from a person moving down the sensor box with a walking speed $v_b = 2.1 \frac{m}{s}$. The working distance between the person and the sensing box is $L = 90 \text{ cm}$. The graph shows *voltage / mV* versus *time / 15 ms*.

6.2 Output signal of four sensor boxes

The four sensor boxes are not installed on the ceiling because an installation of four sensor boxes on the ceiling in the laboratory is not possible. The sensor boxes are installed on the wall. This fact doesn't impact the output signals for this sample application. The sensors are installed in a height of $h = 1.4 \text{ m}$. The working distance between the sensor boxes and the person is $L = 1.3 \text{ m}$ and the distance between two sensor boxes is $s_1 = 1.1 \text{ m}$. To measure the walking speed v_b of the person a stopwatch is used.

Figure 6.4 shows the output signals from a person, moving with a walking speed $v_b = 0.8 \frac{\text{m}}{\text{s}}$. Figure 6.5 shows the output signals from a person, moving with a walking speed $v_b = 1.2 \frac{\text{m}}{\text{s}}$. Figure 6.6 shows the output signals from a person, moving with a walking speed $v_b = 3.1 \frac{\text{m}}{\text{s}}$.

The main differences between the three plots are the amplitude, the signal duration and the time shift between two sensor boxes output signals. The signal form is the same in each plot because the mover is always the same direction.

The different amplitudes are a result of the frequency dependence of the sensor box amplitude transfer. This is explained in the section 6.1. The signal duration depends on the walking speed v_b as also explained in section 6.1.

The time shift Δt between two sensor boxes output signals in Figure 6.5 is about $\Delta t = 57 \text{ samples}$. The duration of one sample is 15 ms . Therefore the time shift between two output signals is $\Delta t = 57 \cdot 15 \text{ ms} = 855 \text{ ms}$. To calculate the walking speed v_b of the person the distance s_1 between two sensors must be divided by the time shift Δt .

$$v_b = \frac{s_1}{\Delta t} = \frac{1.1 \text{ m}}{855 \text{ ms}} = 1.3 \frac{\text{m}}{\text{s}} \quad (6.10)$$

The read off value for the walking speed $v_b = 1.3 \frac{\text{m}}{\text{s}}$ and the measured walking speed $v_b = 1.2 \frac{\text{m}}{\text{s}}$ are very similar. The small difference between the read off value and the calculated value is because the measured walking speed value is not very precise.

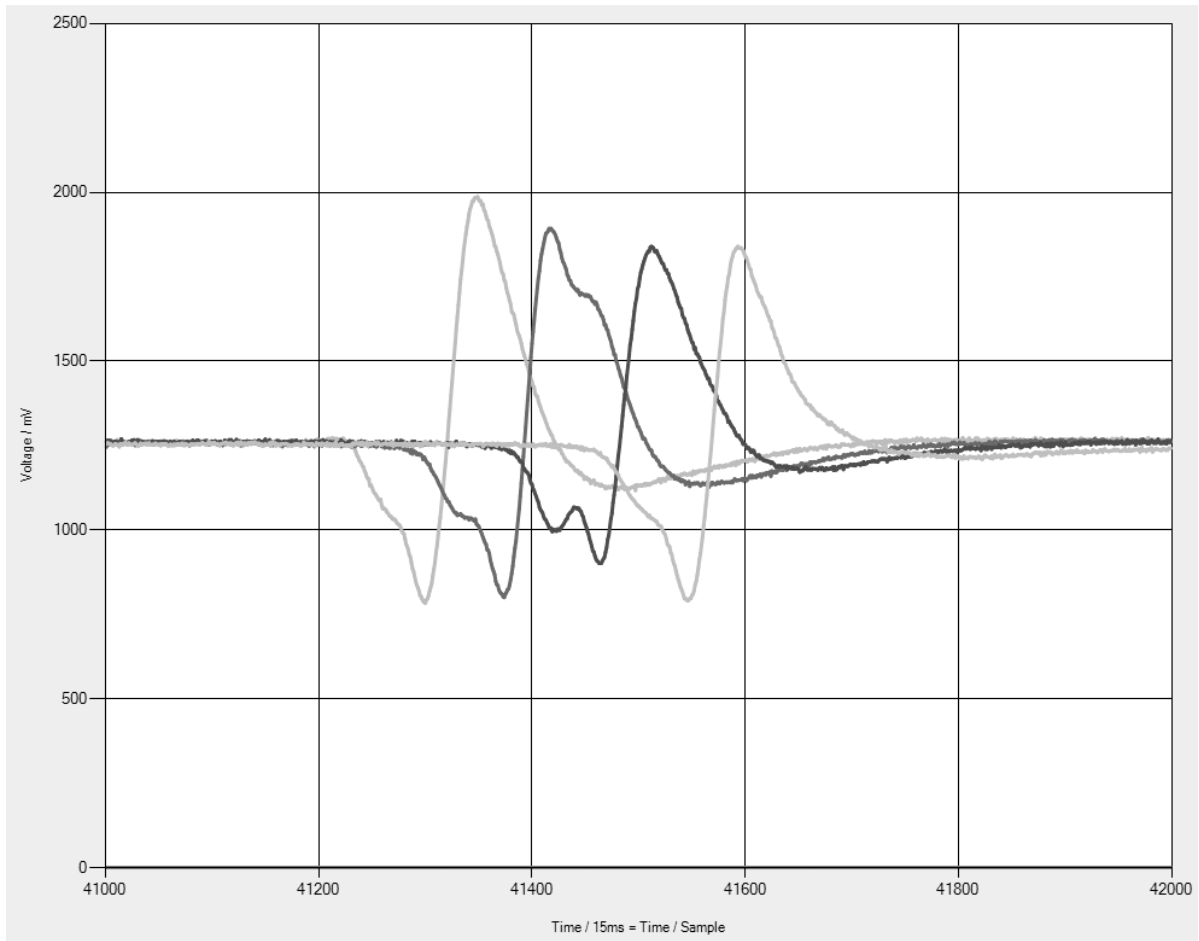


Figure 6.4: Output signal from four sensor boxes while a person walks with a walking speed $v_b = 0.8 \frac{m}{s}$. The distance between two sensor boxes is $s_1 = 1.1 m$. The graph shows *voltage / mV* versus *time / 15 ms*.

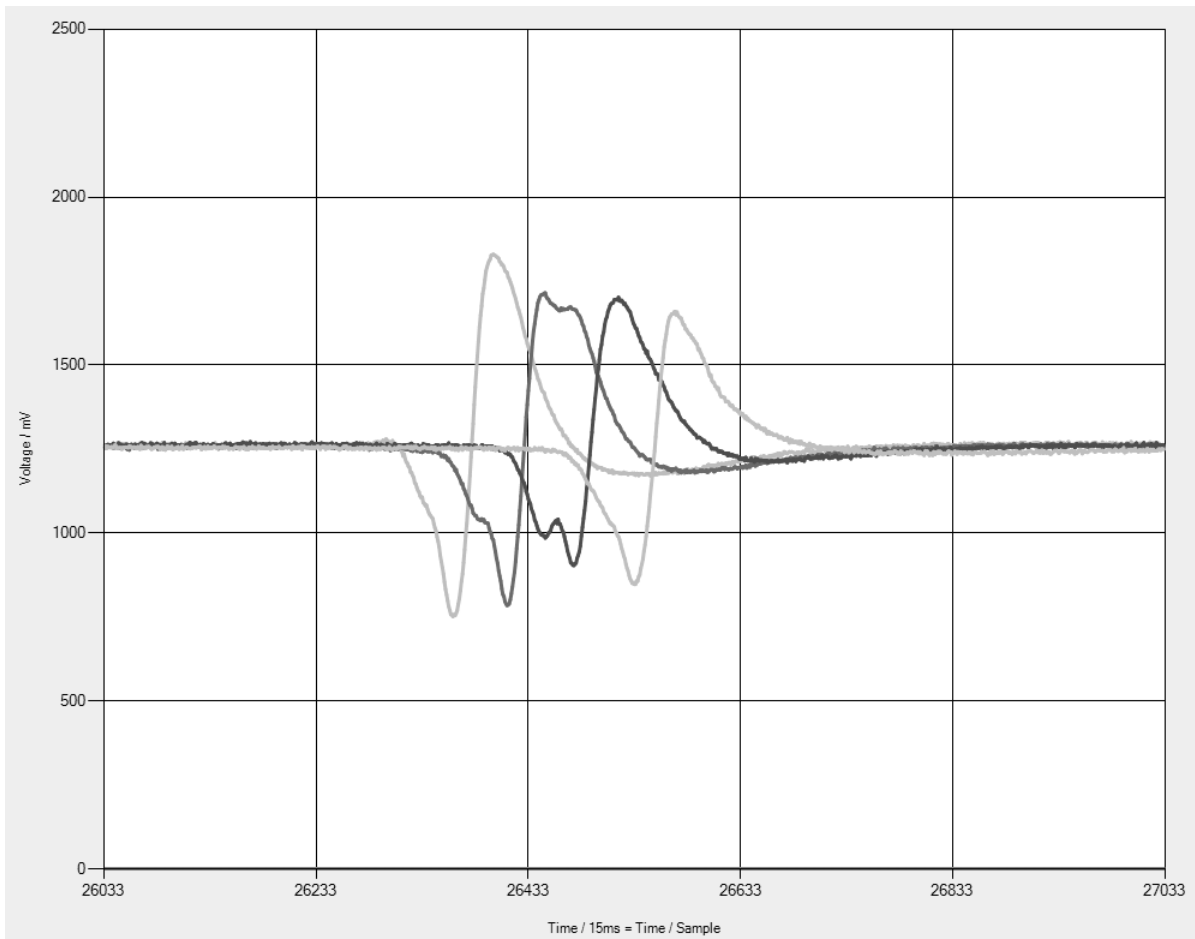


Figure 6.5: Output signal from four sensor boxes while a person walks with a walking speed $v_b = 1.2 \frac{m}{s}$. The distance between two sensor boxes is $s_1 = 1.1 m$. The graph shows *voltage / mV* versus *time / 15 ms*.

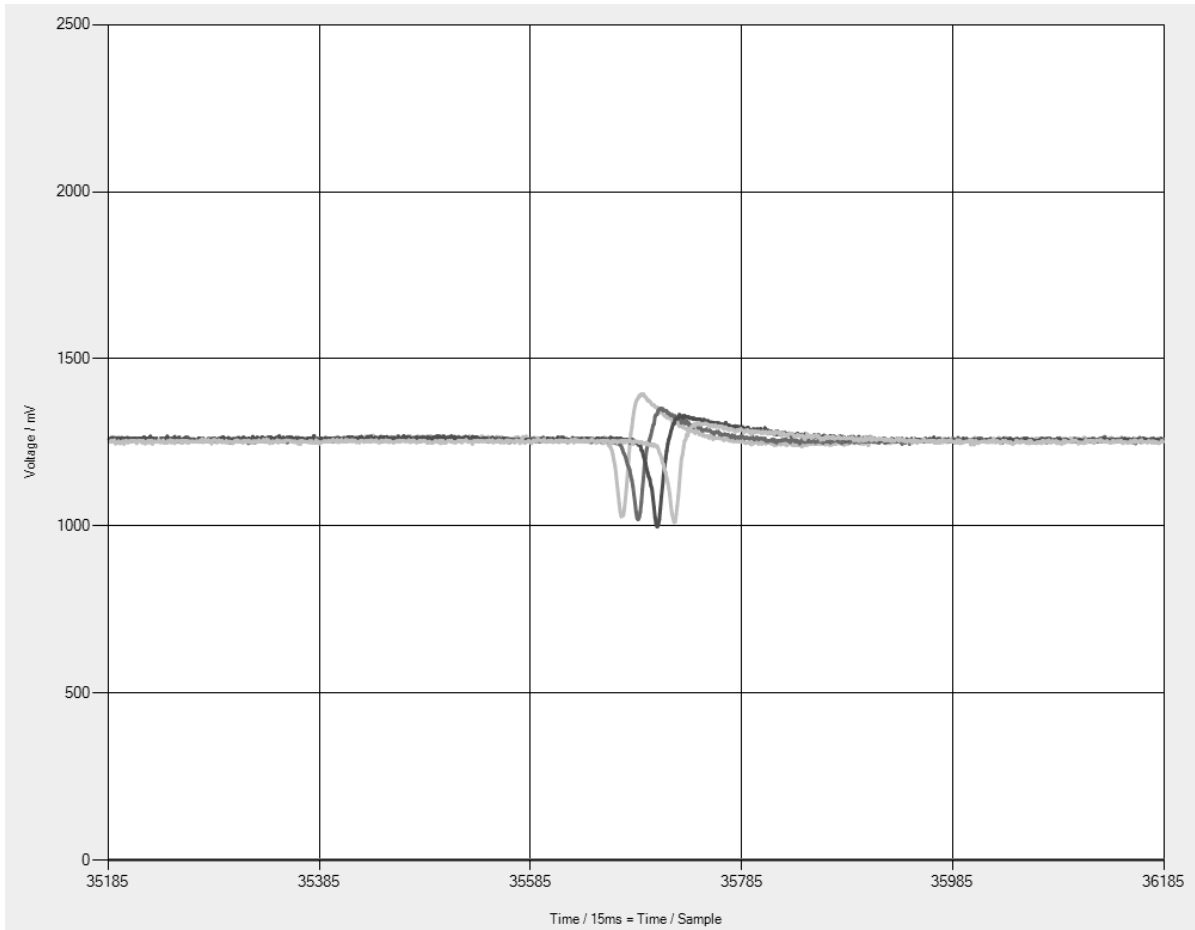


Figure 6.6: Output signal from four sensor boxes while a person walks with a walking speed $v_b = 4.5 \frac{m}{s}$. The distance between two sensor boxes is $s_1 = 1.1 m$. The graph shows *voltage / mV* versus *time / 15 ms*.

7 Conclusion

The first part of this report describes the theory of thermal radiation, detectors for infrared radiation and electrical filters. All this information is the result of an initial background research into different sources of literature.

The second part describes the development of four infrared sensor boxes to detect the infrared radiation emitted by a person. Furthermore, it describes the firmware implemented on a microcontroller to digitise the analogue output signals from the sensor boxes. Finally, it describes the software that has been written to display the signals on a chart on a computer screen in real time.

At the initial stage of the project development, only the microcontroller development kit and the infrared detector were available. To focus the incident infrared radiation on the detector, a suitable lens had to be chosen. In order to interface the sensor to the microcontroller, an analogue filter and amplifier circuit was designed in Eagle and manufactured at Edinburgh Napier University. To digitise the analogue signal, an analogue to digital converter on a microcontroller had to be used. Then firmware was written for the microcontroller. The microcontroller is connected via the serial port to the computer. Furthermore, software was written in Visual Studio 2008 in the programming language C++ to plot the signals in a chart.

During the development process there was a number of problems encountered e.g. the delayed arrival of the external manufactured lens and the time intensive investigation to find an applicable C++ class to present the chart on the computers monitor.

The third part describes two sample applications. In the first application one sensor box was installed on the ceiling, and in the second four sensor boxes were installed on the wall. In both applications, the output signals are shown on the computer and interpreted with the initially described equations and diagrams.

The recorded emitted signals from a human can be combined with algorithms. An algorithm to detect the walking direction from a person, based on the information from one sensor box, is implemented. Algorithms could be developed for other tasks, for example, to record movement profiles of people. The implementation of these algorithms could be done in further investigations and is out of the scope of this thesis.

Bibliography

- [1] F.E. Jones R.A. Smith and R.P. Chasmar. *The detection and measurement of infra-red radiation*. 1968.
- [2] Arpl radiocommunications laboratory. <http://wireless.ictp.it>.
- [3] Jr. Richard D. Hudson. *Infrared System Engineering*. 1969.
- [4] F. A. Sowan. *Applications of Infrared Detectors*. 1971.
- [5] Knut Schmidt-Nielsen. *Animal physiology: adaptation and environment*. 1997.
- [6] W. Larry Kenney Jack H. Wilmore, David L. Costill. *Physiology of Sport and Exercise*. 2008.
- [7] Fresnel Technologies Inc. Poly ir, fresnel lenses for infrared wavelengths. 2000.
- [8] D.Sc. Antonin Vasko. *Infra-red radiation*. 1968.
- [9] Mool C. Gupta and John Ballato. *Handbook of Photonics*. 2007.
- [10] Prof L. J. Gauckler and Prof. K. Conder. Ceramics ii. Technical report, ETH Zuerich.
- [11] R W Whatmore. Pyroelectric devices and materials. Technical report, Allen Clark Research Centre.
- [12] InfraTec. Detector basics. Application note.
- [13] PerkinElmer optoelectronics. *Dual element detector LHi 954/958*, 2001.
- [14] Wikimedia commons. <http://commons.wikimedia.org>.
- [15] PerkinElmer. Closeup 1/02, frequency range for pyroelectric detectors. 2002.
- [16] Silicon Laboratories. *C8051F35x Development kit user's guide*, 2006.
- [17] Silicon Laboratories. *C8051F350/1/2/3*, 2007.

BIBLIOGRAPHY

- [18] Microsoft developer network. <http://msdn.microsoft.com>.
- [19] Microsoft download center. <http://www.microsoft.com/downloads>.
- [20] George Clayton and Bruce Newby. *Operational Amplifiers*. 1992.